



Long noncoding RNA *LncBAR* enhances BRG1 protein to promote cardiomyocyte cell cycle progression and cardiac repair



Jun Li^{1,2,5}, Huanhuan Cai^{1,2,3,5}, Yufan Chen^{1,2}, Ruiqi Pi¹, Lilin Xiang^{1,2,3}, Zhibing Lu^{1,2,3}✉, Yan Zhou⁴✉ & Li Wang^{1,2}✉

The mammalian heart retains regenerative capacity during the early postnatal period, but this ability declines as it matures. Enhancing cardiomyocyte proliferation represents a key therapeutic approach to promote heart regeneration and repair, yet the molecular mechanisms remain elusive. Here, we identified *LncBAR* (BAF complex-associated lncRNA) as a critical regulator of cardiac regeneration. *LncBAR* expression declines during heart development but is upregulated following cardiac injury. Loss of *LncBAR* impairs cardiomyocyte growth, suppresses cell cycle gene expression, and diminishes heart regeneration, as evidenced by reduced cytokinesis and cardiac function. Conversely, cardiac specific overexpression of *LncBAR* restores cardiomyocyte proliferation and enhances cardiac regeneration, especially in adult myocardial infarction model. Mechanistically, *LncBAR* interacts with *Brg1*, stabilizing BRG1 protein level and activating cell cycle progression to drive cardiomyocytes proliferation. Collectively, our study identified *LncBAR* as a crucial regulator for heart regeneration, highlighting the *LncBAR*-BRG1 axis as a promising therapeutic strategy for cardiac repair.

Heart disease results in massive loss of cardiomyocytes (CMs) and is among the leading causes of morbidity and mortality worldwide. Due to the limited regenerative capacity of adult mammalian hearts, the infarcted heart fails to generate new CMs to replenish those lost during injury, leading to cardiac remodeling and eventually heart failure^{1–3}. In contrast, the neonatal mammalian heart possesses a transient regenerative capacity through cardiomyocyte proliferation that is limited to the first week after birth and is lost shortly thereafter^{4–6}. Growing evidence suggests that inducing adult CM re-entry into the cell cycle can remuscularize the injured myocardium and promote cardiac repair^{7–10}. Therefore, deciphering the regulators and molecular mechanisms that stimulate CM proliferation holds promising potential for developing therapeutic strategies to treat ischemic heart diseases in adults.

The Switch/Sucrose Non-Fermentable (SWI/SNF) complex is an ATP-dependent chromatin remodeling complex that changes the accessibility of transcription factors to DNA¹¹. Among its multiple subunits, the essential ATPase subunit *Brg1* (also known as *Smarca4*)¹² plays critical roles in cardiac growth and differentiation

under developmental and pathological conditions^{13–15}. During zebrafish heart regeneration, BRG1 interacts with DNA methyltransferase *Dnmt3ab* to suppress cyclin-dependent kinase inhibitors, such as *Cdkn1c*, thereby promoting the CM proliferation¹⁶. In mammalian heart, BRG1 expression is typically silenced in adult CMs but can be reactivated in response to cardiac stresses¹⁴. Recent studies have shown that forced expression of BRG1 protects heart from acute myocardial infarction by reducing oxidative damage and cell apoptosis¹⁵. Despite its biological significance, the regulatory mechanisms governing BRG1 expression remain largely unknown.

Long noncoding RNAs (lncRNAs) are nonprotein coding transcripts longer than 200 nucleotides¹⁷. Recent studies have demonstrated that lncRNAs play crucial roles in various cardiovascular diseases^{18–23}. lncRNAs regulates gene expression at multiple levels, including transcription, RNA splicing and protein translation to participate in the cardiac remodeling and regeneration. We recently identified an intergenic lncRNA termed *LncBAR* that binds with SWI/SNF complex, particularly with BRG1, to regulate neocortical development²⁴. However, the contribution of *LncBAR* in the

¹Department of Cardiology, Medical Research Institute, Zhongnan Hospital of Wuhan University; Frontier Science Center for Immunology and Metabolism, Wuhan University, Wuhan, China. ²Institute of Myocardial Injury and Repair, Wuhan University, Wuhan, China. ³Hubei Provincial Clinical Research Center for Cardiovascular Intervention, Wuhan, China. ⁴Hubei Provincial Research Center for Basic Biological Sciences; Department of Stomatology, Medical Research Institute, Zhongnan Hospital of Wuhan University; Frontier Science Center of Immunology and Metabolism, Wuhan University, Wuhan, China. ⁵These authors contributed equally: Jun Li, Huanhuan Cai. ✉e-mail: luzhibing@whu.edu.cn; yan.zhou@whu.edu.cn; liwang2020@whu.edu.cn

regulation of cardiac regeneration and its association with BRG1 remain less understood.

In this study, we investigated the role of *LncBAR* in cardiomyocyte proliferation and postnatal cardiac regeneration. *LncBAR* deficiency blocked cardiomyocyte proliferation and impaired cardiac function recovery after apical resection (AR). In contrast, overexpressing *LncBAR* enhanced cardiac regeneration and post-AR heart functions. Mechanistically, *LncBAR* stabilized BRG1 protein levels, thereby stimulating cell cycle progression and promoting cardiomyocyte proliferation. Collectively, our results revealed that *LncBAR* acts as an activator of cardiomyocyte proliferation and present a promising strategy to enhance cardiac repair.

Results

LncBAR regulates murine neonatal cardiomyocyte proliferation

To investigate the potential role of *LncBAR* in heart regeneration, we assessed *LncBAR* expression levels in the hearts across different developmental stages, from embryo (embryonic day 13.5) to adulthood (12 weeks old), using quantitative reverse transcription-polymerase chain reaction (RT-qPCR). We observed that, under physiological conditions, *LncBAR* expression gradually decreased during cardiac development (Fig. 1a). Following apical resection (AR) in wild-type (WT) mice at day 1 (P1), *LncBAR* levels increased specifically in the apical zone (AZ) at both d7 and d21 post-AR (AR7 and AR21), compared to the border and remote zones (BZ and RZ) (Fig. 1b). Furthermore, following myocardial infarction (MI), *LncBAR* expression was markedly increased in the infarct zone (IZ) and moderately upregulated in the border zone (BZ) (Fig. 1c). These results suggested a positive correlation between *LncBAR* expression and cardiac regeneration, prompting us to further investigate its role in the postnatal heart.

To explore this, we designed lentivirus encoding a panel of short hairpin RNA (shRNA) targeting *LncBAR* and the knockdown efficiency achieved approximately 80–90% (Supplementary Fig. 1a). Importantly, knocking down *LncBAR* had minimal effect on the expression of its two neighboring genes, *Zfp207* and *Psm11* in the neonatal mouse cardiomyocytes (NMCMs) (Supplementary Fig. 1b). We then performed immunofluorescence staining (ICC) against cTnI, a marker of cardiomyocytes and 5-ethynyl-2'-deoxyuridine (EdU), a nucleotide analog that labels cells passing through the S phase, at 4 days post viral infection (Fig. 1d). ICC results indicated that *LncBAR* knockdown significantly reduced the number of EdU+ cardiomyocytes and total cardiomyocytes (Fig. 1e), suggesting that *LncBAR* may regulate NMCM proliferation. Individual sh*LncBAR* oligonucleotides showed similar suppression effects on NMCM proliferation as pooled oligonucleotides. For the rest of the study, we used pooled sh*LncBARs* (referred to as sh*LncBAR*) unless otherwise indicated (Supplementary Fig. 1c).

We next performed gain-of-function experiments by delivering lentiviral *LncBAR* overexpression construct into NMCMs. Lentiviruses carrying LacZ fragment were used as control, and PBS was used as non-viral treatment control. Transduction efficiency, assessed via GFP, increased with MOI from 25 (~20% transduction, ~20-fold *LncBAR* expression) to 100 (~94% transduction, ~250-fold expression). Overexpression at MOI 50 significantly increased the number of Ki67+ cardiomyocytes, which was further enhanced at MOI 100. Therefore, MOI 100 was used in all subsequent in vitro experiments (Supplementary Fig. 1d–f).

Overexpression of *LncBAR* in NMCMs remarkably elevated EdU-positive cardiomyocytes (Fig. 1f). We used another active proliferation marker, Ki67, and cardiac troponin I (cTnI) to mark proliferating CMs. Congruently, we observed an increase in the number of both cTnI+ NMCMs and Ki67+ cTnI+ proliferating NMCMs after *LncBAR* overexpression (Fig. 1g). We also used marker of cytokinesis (Aurora B) and cTnI. The results showed that overexpression of *LncBAR* significantly increased the number of Aurora B+ CMs and total CMs (Fig. 1h). Furthermore, we conducted propidium iodide (PI) staining in *LncBAR*-overexpressing HL-1 cardiomyocytes, which showed a significant shift from G0/G1 to S and G2/M phases, indicating enhanced cell cycle progression (Supplementary Fig. 1g). To assess actual cell division, we quantified

NMCM numbers on day 4 after *LncBAR* or control lacZ overexpression, and found a significant increase in cardiomyocyte counts following *LncBAR* overexpression (Supplementary Fig. 1h). At the transcription level, RT-qPCR analyses showed that sh*LncBAR* treatment significantly down-regulated genes positively regulating the cell cycle and cell proliferation (Fig. 1i), while *LncBAR* overexpression increased the expression of these genes (Fig. 1j). Collectively, our data indicate that *LncBAR* plays a key role in regulating NMCM proliferation.

LncBAR depletion inhibits cardiomyocyte proliferation in postnatal hearts

To investigate the role of *LncBAR* in vivo, we generated *LncBAR* knockout (KO) mice (Fig. 2a) using a CRISPR/Cas9-mediated gene editing approach²⁴. Genotyping results confirmed successful *LncBAR* depletion (Fig. 2b), and RT-qPCR analysis validated deficient expression of *LncBAR* in KO hearts compared with controls (Fig. 2c). We assessed CM proliferation in *LncBAR* KO and WT hearts at postnatal days P3 and P7. *LncBAR* depletion remarkably inhibited the proliferation of CMs at P3 and P7, as indicated by co-staining of cTnT with mitosis markers including phosphohistone H3 (pH3) and Ki67 (Fig. 2d–g).

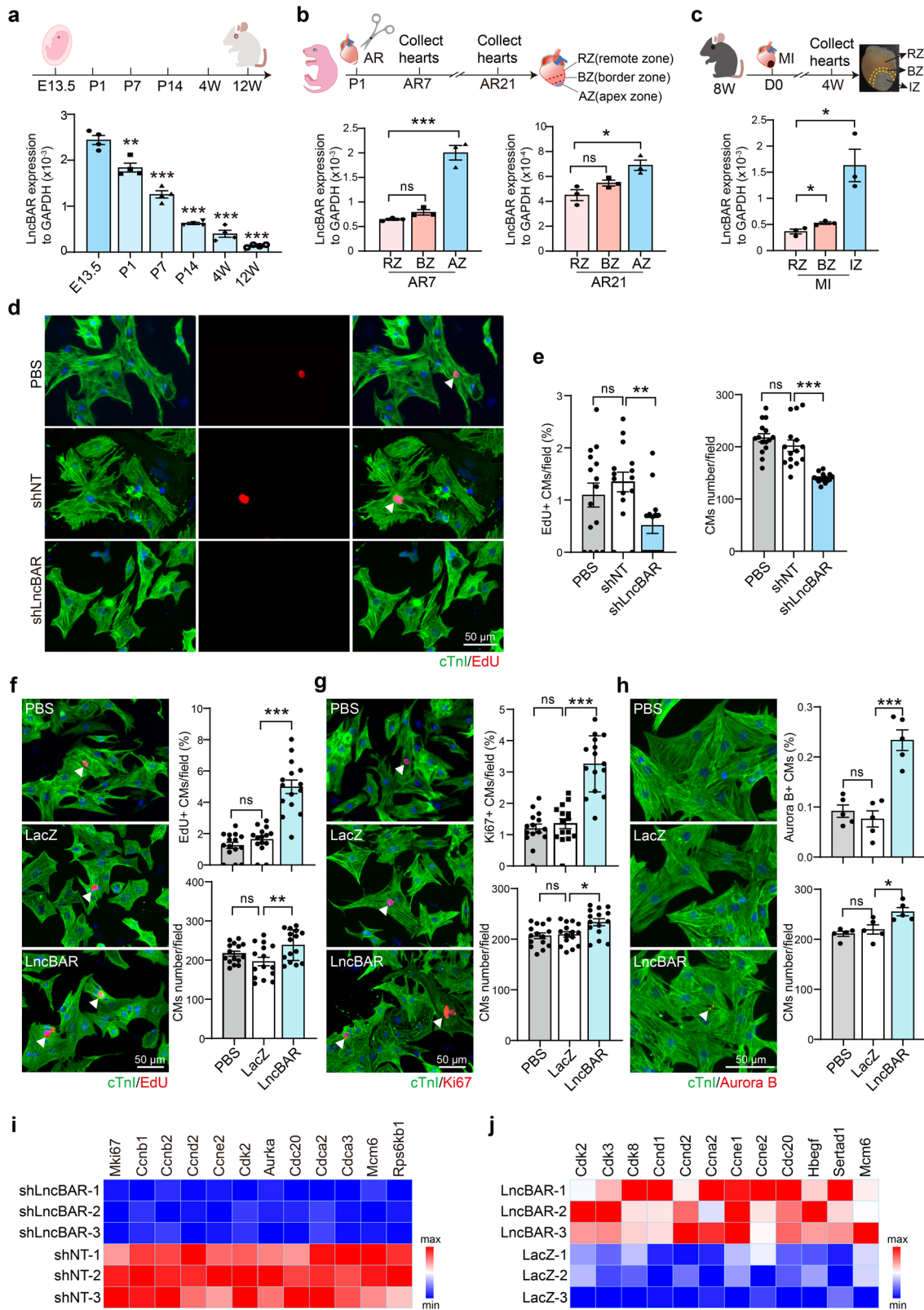
To evaluate whether the effects of *LncBAR* are cardiomyocyte-specific, we examined its expression across cardiac cell types. RT-qPCR on sorted neonatal heart cells showed that *LncBAR* expression was significantly higher in NMCMs compared to cardiac fibroblasts (CFs) and endothelial cells (ECs) (Supplementary Fig. 2a). We next investigated the effects of *LncBAR* depletion in non-myocytes, achieving ~50% knockdown in CFs and ~85% in ECs (Supplementary Fig. 2b, c). Functional assays revealed that *LncBAR* knockdown did not significantly alter fibroblast proliferation or number, as assessed by vimentin and pH3 staining, nor did it affect EC proliferation or total cell counts (Supplementary Fig. 2d, e). Together, these data indicate that *LncBAR* is enriched in cardiomyocytes and exerts minimal effects on CFs and ECs under homeostatic conditions.

We then examined whether reduced cardiomyocyte proliferation affects heart function in *LncBAR* KO adult mice. Echocardiography showed minor differences in left ventricular ejection fraction (LVEF), left ventricular fractional shortening (LVFS), left ventricular end-diastolic volumes (LVEDV), left ventricular end-systolic volumes (LVESV), stroke volume (SV) and heart rate (HR) between *LncBAR* KO and WT mice (Supplementary Fig. 2f–l). However, the heart-to-body weight ratio was slightly lower in *LncBAR* KO mice (Supplementary Fig. 2m, n). Wheat germ agglutinin (WGA) staining showed reduced cardiomyocyte size compared to controls (Supplementary Fig. 2o). Additionally, isolated cardiomyocytes from adult *LncBAR* KO mice had a smaller area than those from WT mice (Supplementary Fig. 2p). These results suggest that adult *LncBAR* KO mice may reduce the heart size to compensate for the proliferation defects during the neonatal stage.

LncBAR depletion inhibits neonatal heart regeneration

Next, we investigated whether *LncBAR* deficiency undermines tissue regeneration in early postnatal hearts. We subjected *LncBAR* KO mice and their littermate WT counterparts to AR at P1. Heart samples were collected at AR7 and AR21 for histological and functional analyses (Fig. 3a). ICC on heart sections taken at AR7 revealed a reduced number of Ki67-positive and pH3-positive cardiomyocytes in *LncBAR* KO hearts compared to WT hearts (Fig. 3b, c). Additionally, Masson's trichrome staining showed a significant increase in fibrotic area in *LncBAR* KO hearts at AR7 compared with WT hearts (Fig. 3d). Consistently, while neonatal WT hearts regenerated well with barely detectable fibrosis at AR21, *LncBAR* KO hearts exhibited significant fibrosis and more pronounced reductions in heart functions at AR21 (Fig. 3e–g), highlighting the pivotal role of *LncBAR*.

To exclude potential developmental defects arising from *LncBAR* KO that might affect heart regeneration, we delivered sh*LncBAR* and shNT control viruses into newborn hearts and performed AR surgery on P1. Hearts were collected at AR7 (Supplementary Fig. 3a). RT-qPCR results confirmed that viral injection decreased cardiac *LncBAR* expression by 50%



(Supplementary Fig. 3b). ICC of hearts treated with sh*LncBAR* demonstrated a significant reduction in Ki67+ and pH3+ proliferative cardiomyocytes (Supplementary Fig.3c, d). These findings collectively suggest that *LncBAR* depletion attenuates cardiomyocyte proliferation and compromises heart regeneration.

***LncBAR* overexpression promotes cardiomyocyte regeneration and improves cardiac functions after myocardial injury**

To investigate whether increased expression of *LncBAR* could extend the cardiac regenerative potential, we introduced exogenous *LncBAR* into mice using an adeno-associated virus serotype 9 (AAV9)-mediated delivery

Fig. 1 | Long non-coding RNA (*LncBAR*) regulates cardiomyocyte proliferation.

a Quantitative reverse transcription-polymerase chain reaction (RT-qPCR) analysis of *LncBAR* expression in murine hearts at indicated time points (embryonic day (E) 13.5; postnatal days (P) 1 to P14, and 4 and 12 weeks (W)) ($n = 4$ mice). **b** Relative *LncBAR* expression in hearts at 7 (AR7) and 21 (AR21) days post-apical resection (AR), determined by RT-qPCR. RZ: remote zone; BZ: border zone; AZ: apex zone ($n = 3$ mice). **c** Relative *LncBAR* expression in murine hearts at 4 weeks post-myocardial infarction (MI) by RT-qPCR. RZ: remote zone; BZ: border zone; IZ: infarct zone. ($n = 3$ mice). **d** ICC analysis of EdU-incorporated NMCMs for cTnI (cardiomyocyte marker). Cells were transduced with sh*LncBAR*, control shNT, or PBS and cultured with EdU for 1 day prior to staining. White arrows indicate EdU+ NMCMs. Scale bars, 50 μm . **e** Proportions of total (cTnI+) and proliferating (EdU+ cTnI+) NMCMs 4 days after treatment with sh*LncBAR*, shNT, or PBS. ($n = 15$ fields). **f** Representative ICC and quantification of cTnI+ cells in EdU-incorporated

NMCMs following transduction with lentivirus harboring LacZ or *LncBAR*, or treatment with PBS (vehicle control), after a 24 h EdU pulse. White arrows indicate EdU+ NMCMs ($n = 15$ fields). Scale bars, 50 μm . **g** Representative ICC and quantification of cTnI and Ki67 in NMCMs treated with or without lentiviral *LncBAR*. PBS was used as non-viral treatment control. White arrows indicate Ki67+ NMCMs ($n = 15$ fields). Scale bars, 50 μm . **h** Representative ICC and quantification of cTnI and Aurora B in NMCMs treated with or without lentiviral *LncBAR*. PBS was used as non-viral treatment control. White arrows indicate Aurora B+ NMCMs ($n = 5$ biological replicates). Scale bars, 50 μm . **i, j** RT-qPCR analysis showing the expression of genes positively regulating the cell cycle and proliferation upon *LncBAR* knockdown (**i**) or overexpression treatment (**j**) ($n = 3$ biological replicates). Data are presented as mean \pm SEM. Statistical significance was determined by one-way ANOVA with Tukey's multiple comparisons test. * $P < 0.05$, ** $P < 0.01$, *** $P < 0.001$.

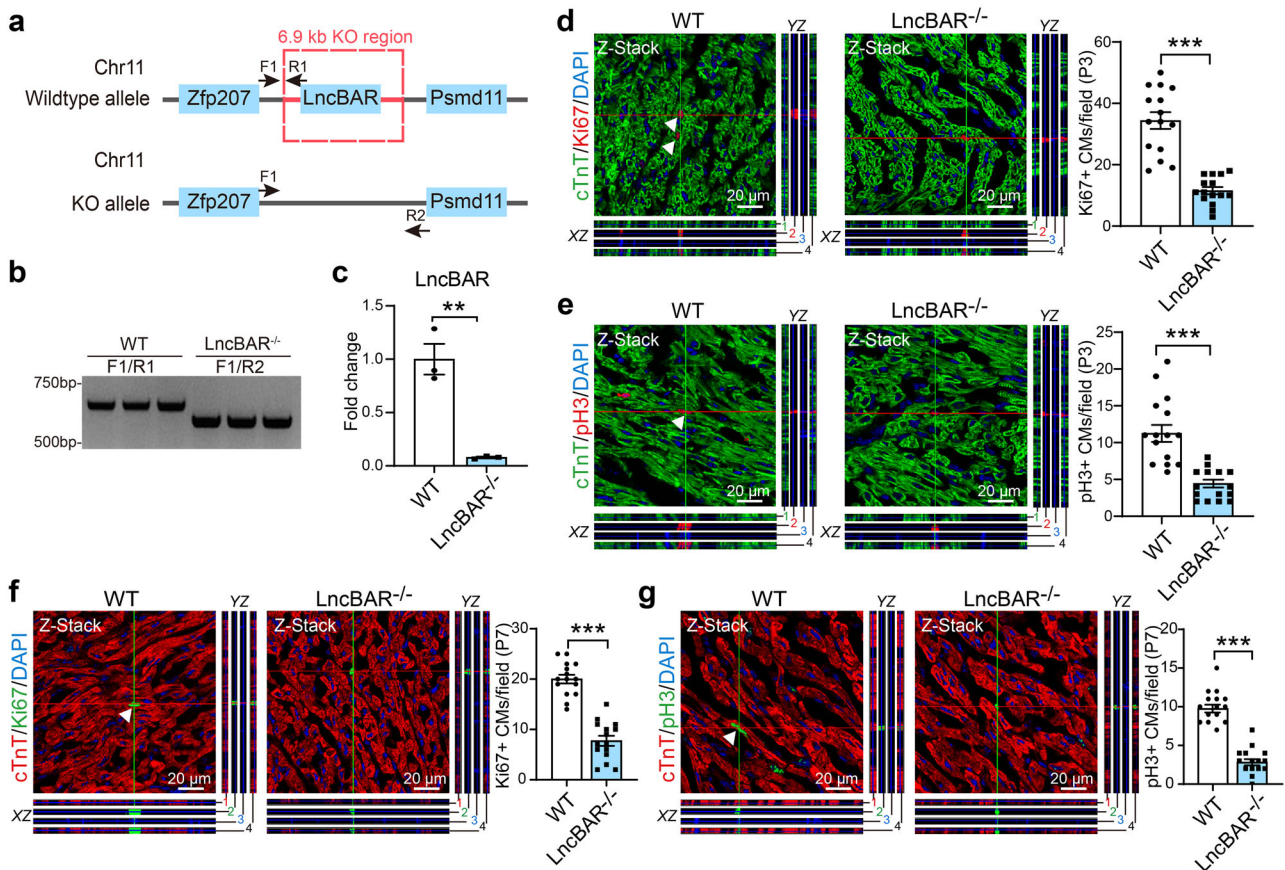


Fig. 2 | *LncBAR* deficiency inhibits cardiomyocyte proliferation in postnatal hearts. **a** Schematic depiction of *LncBAR* knockout (KO) mice and the genotyping strategy. F and R, primers designed for genotyping. **b** Representative genotyping results from wild-type and *LncBAR* KO (*LncBAR*^{-/-}) mice using PCR primer pairs shown in (a) ($n = 3$ mice). **c** Expression level of *LncBAR* in WT and *LncBAR*^{-/-} hearts as evaluated by RT-qPCR ($n = 3$ mice). Representative confocal z-stack images and quantification of cTnT+ Ki67+ (d) or cTnT+ pH3+ CMs (e) in heart sections from neonatal WT and *LncBAR*^{-/-} hearts at P3. Nuclei were labeled with DAPI. White

arrows indicate Ki67+ or pH3+ CMs ($n = 15$ fields, 3 mice/group). Scale bars, 20 μm . **f, g** Representative confocal z-stack images and quantification of cTnT+ Ki67+ (f) or cTnT+ pH3+ CMs (g) in heart sections from neonatal WT and *LncBAR*^{-/-} hearts at P7. Nuclei were labeled with DAPI. White arrows indicate Ki67+ or pH3+ CMs ($n = 15$ fields, 3 mice/group). Scale bars, 20 μm . Data are presented as mean \pm SEM. Statistical significance was determined by two-tailed unpaired *t* test. ** $P < 0.01$, *** $P < 0.001$.

system^{25,26}. Newborn mice were intramyocardially injected with AAV9-cTnT-*LncBAR* or AAV9-cTnT-GFP control viruses, with expression driven by cardiomyocyte-specific cTnT promoter. Saline-treated group was used as non-viral control. AR injury was performed at non-regenerative stage (P8), and heart tissues were collected at AR7 and AR21 for histological and functional analyses (Fig. 4a). We evaluated the transduction efficiency of the applied AAVs by quantifying GFP-positive cardiomyocytes, which reached approximately 83% in the AAV9-cTnT-GFP group (Fig. 4b), indicating that

the majority of cardiomyocytes were successfully transduced. Overexpression of *LncBAR* was verified by RT-qPCR in AAV9-cTnT-*LncBAR* hearts (Fig. 4c). Co-immunostaining of cTnT with proliferation markers in heart sections showed that *LncBAR* overexpression significantly increased the number of Ki67+ and pH3+ cardiomyocytes after AR injury compared with controls (Fig. 4d, e). Masson's trichrome staining of heart sagittal sections collected at AR7 and AR21 both showed that overexpression of *LncBAR* led to reduced scar size in the apical injury zone compared with

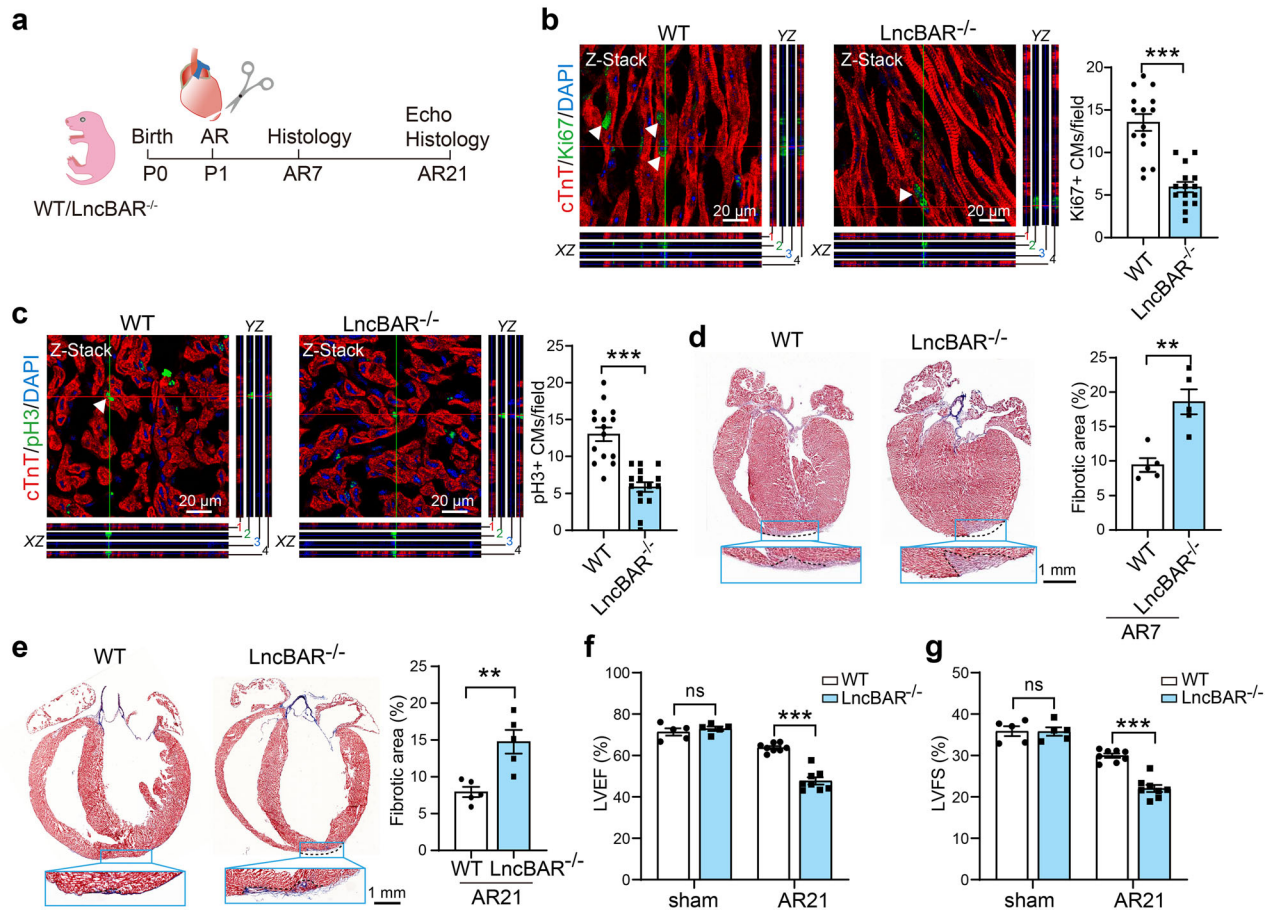


Fig. 3 | *LncBAR* depletion inhibits neonatal heart regeneration. **a** Schematic depiction of the experimental design in WT and *LncBAR*^{-/-} neonatal mice. **b, c** Representative confocal z-stack images and quantification of Ki67+ cTnT+ CMs (**b**), and pH3+ cTnT+ CMs (**c**) from WT and *LncBAR*^{-/-} heart sections in the apex zone at day 7 after AR (AR7). White arrows indicate Ki67+ or pH3+ CMs ($n = 15$ fields, 3 mice/group). Scale bars, 20 μm. Masson's trichrome staining and quantification of fibrotic area (blue) in sagittal heart sections from WT and

LncBAR^{-/-} mice at AR7(**d**) and AR21(**e**) ($n = 5$ mice). Scale bars, 1 mm. Echocardiography showing left ventricular ejection fraction (**f**) and fractional shortening (**g**) at AR21 of WT and *LncBAR*^{-/-} mice ($n = 5$ mice for sham groups, $n = 8$ mice for AR groups). Data are presented as mean ± SEM. Statistical significance was determined by two-tailed unpaired *t* test or two-way ANOVA with Tukey's multiple comparisons test. ** $P < 0.01$, *** $P < 0.001$.

control groups (Fig. 4f, g). While AR resulted in significant reduction in heart functions, *LncBAR* overexpression contributed to significantly improved LVEF and LVFS (Fig. 4h–j). These results suggest that elevating *LncBAR* expression levels can protect the heart from AR-induced injury by promoting cardiomyocyte proliferation.

***LncBAR* overexpression enhanced adult cardiac regeneration and functional recovery**

We next investigated whether *LncBAR* plays a functional role in regulating adult heart repair. We performed both loss- and gain-of-function experiments in adult (8-week-old) mice subjected to MI via left anterior descending coronary artery (LAD) ligation. Specifically, we used *LncBAR* knockout (KO) and wild-type (WT) mice to examine the effects of *LncBAR* loss, and concurrently administered AAV9-cTnT-*LncBAR* or control viruses during MI surgery to evaluate the gain-of-function effects. Importantly, the gain-of-function approach also served as a rescue experiment, as *LncBAR* overexpression in KO mice was tested for its ability to restore impaired cardiac repair. Cardiac function was assessed longitudinally by echocardiography at weekly intervals post-MI, and hearts were collected for histological and immunohistochemical analyses at 2- and 6-week post-injury (Fig. 5a). The data demonstrated a significant increase in total cardiomyocyte number per heart at 2 weeks post-injury in *LncBAR*-treated mice compared to controls (Fig. 5b).

Importantly, we observed an increase in the proportion of mono-nucleated cardiomyocytes accompanied by a corresponding decrease in binucleated and multinucleated cardiomyocytes in the *LncBAR* group (Fig. 5c), indicating an expanded subpopulation of cardiomyocytes undergoing cytokinesis.

Wheat germ agglutinin (WGA) staining revealed that cardiomyocytes in *LncBAR*-overexpressing hearts exhibited significantly reduced cross-sectional area, effectively reversing the hypertrophic enlargement observed in *LncBAR* KO mice (Supplementary Fig. 4a). Immunocytochemistry revealed an increase in Aurora B+, Ki67+, and pH3+ cardiomyocytes following *LncBAR* overexpression, which rescued the proliferation deficits caused by *LncBAR* deletion (Fig. 5d–f). Furthermore, Masson's trichrome staining at 6 weeks post-MI showed that *LncBAR* knockout significantly exacerbated fibrotic scar formation, whereas *LncBAR* overexpression attenuated fibrosis and rescued the detrimental effects of *LncBAR* loss (Fig. 5g, h). Echocardiographic assessments revealed no significant differences in cardiac function between groups under baseline conditions. However, after MI, *LncBAR* overexpression markedly improved cardiac function and reversed the impairment induced by *LncBAR* knockout. This functional benefit was sustained through 6 weeks post-MI (Fig. 5i, j and Supplementary Fig. 4b, c). Collectively, these data demonstrate that *LncBAR* promotes cardiomyocyte proliferation, reduces fibrosis, and improves cardiac performance following MI in adult mice.

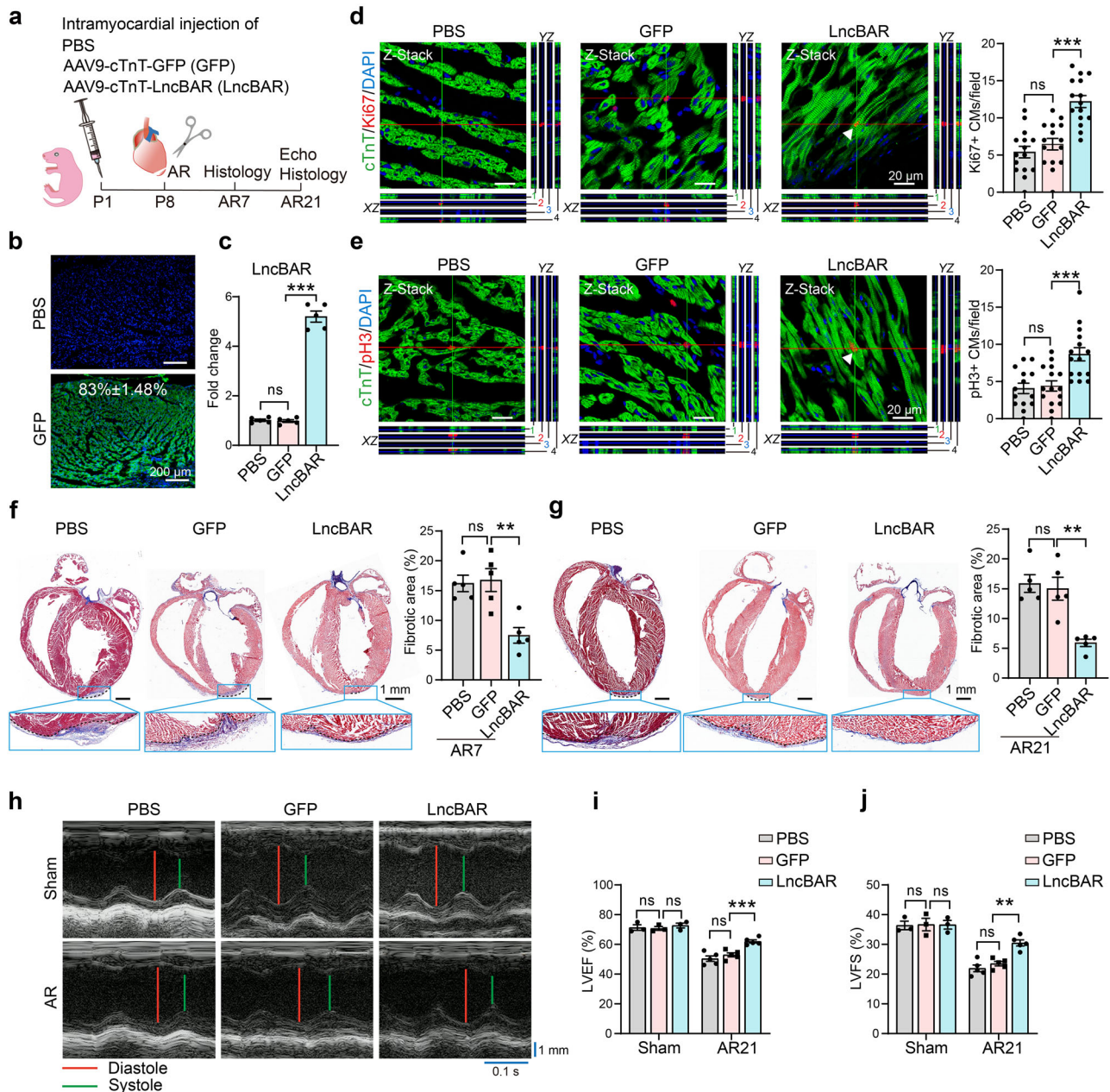


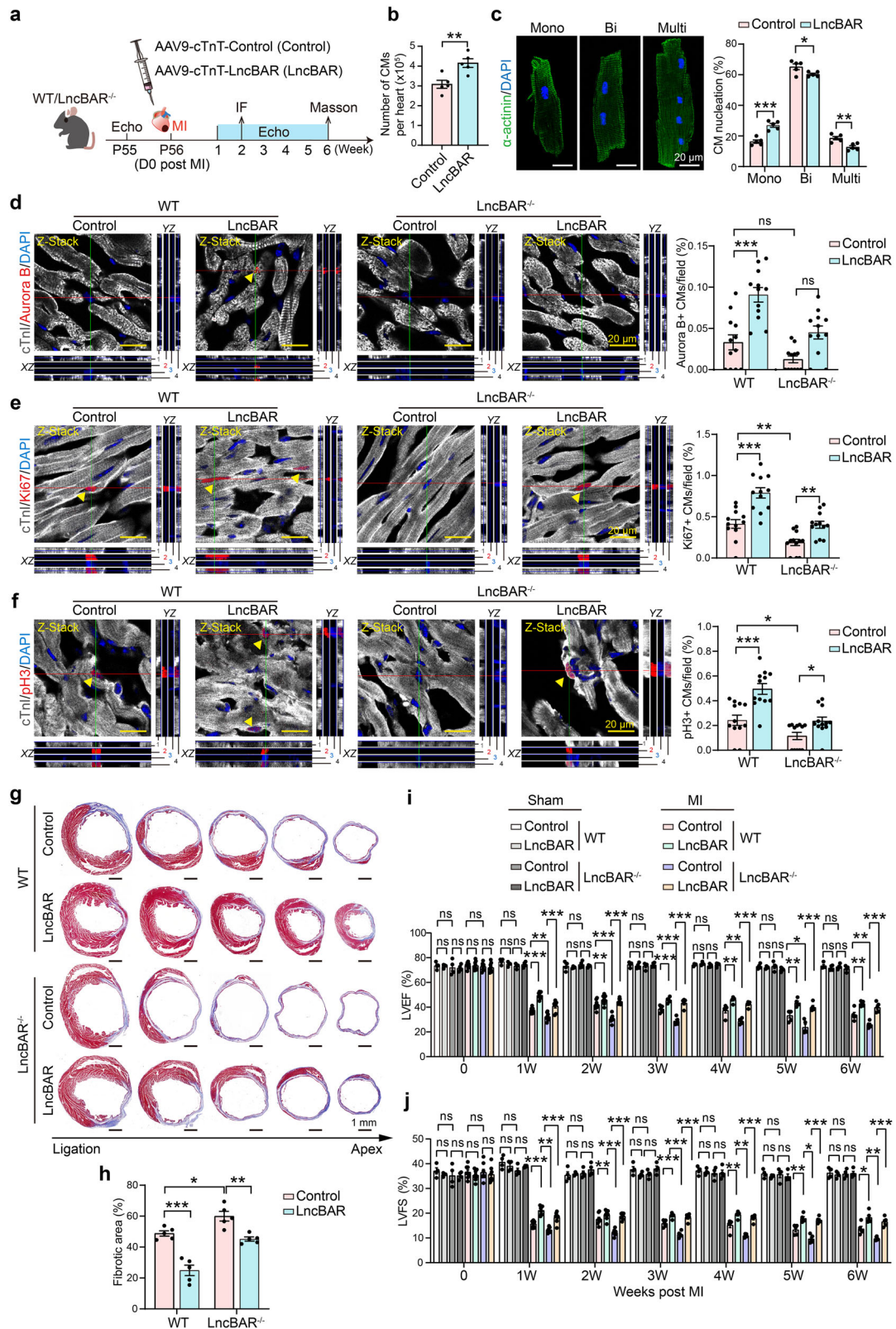
Fig. 4 | *LncBAR* overexpression enhances cardiomyocyte proliferation after AR injury. **a** Schematic depiction of AR experiments. Adeno-associated virus serotype 9 (AAV9) with *LncBAR* overexpression driven by cardiac specific promoter cTnT (AAV9-cTnT-*LncBAR*) or control virus expressing GFP (AAV9-cTnT-GFP) were intramyocardially injected into the neonatal mice hearts. The PBS group was used as a non-viral control. AR surgery was performed at P8, echo and histology samples were collected at AR7 and AR21. **b** Quantification analysis of the transduction efficiency of adeno-associated viruses by the percentage of GFP+ cells. Scale bars, 200 μ m. **c** RT-qPCR analysis showing the expression level of *LncBAR* in hearts receiving AAV9-cTnT-*LncBAR* virus. AAV9-cTnT-GFP injected hearts were used as control. PBS injected hearts were used as non-viral control ($n = 5$ mice). Representative confocal z-stack images and quantification of Ki67+ cTnT+ CMs (**d**), and

pH3+ cTnT+ CMs (**e**) in the cryosection of apex zone of hearts receiving AAV9-cTnT-*LncBAR* or AAV9-cTnT-GFP or PBS injection at AR7. White arrows indicate proliferating CMs ($n = 15$ fields, 3 mice/group). Scale bars, 20 μ m. Masson's trichrome staining and quantification of cardiac fibrosis in heart sagittal sections from AAV9-cTnT-*LncBAR*, AAV9-cTnT-GFP and PBS mice at AR7 (**f**) and AR21 (**g**) ($n = 5$ mice). Scale bars, 1 mm. **h** Echocardiography assessing left ventricular function at AR21 in mice treated with AAV9-cTnT-*LncBAR*, AAV9-cTnT-GFP, or PBS. Quantification of left ventricular ejection fraction (**i**) and fractional shortening (**j**) at 3 weeks after AR in AAV9-cTnT-*LncBAR* and control mice ($n = 3$ mice for sham groups and $n = 5$ mice for AR groups). Data are presented as mean \pm SEM. Statistical significance was determined by one-way or two-way ANOVA with Tukey's multiple comparisons test. ** $P < 0.01$, *** $P < 0.001$.

Activation of PI3K-AKT pathway during *LncBAR*-induced cardiomyocyte survival and proliferation

To profile the transcriptional regulatory effects of *LncBAR* in cardiomyocytes, RNA sequencing (RNA-seq) was employed under conditions of *LncBAR* knockdown and control (Fig. 6a). We identified 1,694 differentially expressed genes (DEGs) in sh*LncBAR*-treated NMCs ($P < 0.05$, |fold change| ≥ 2) (Fig. 6b). Among them, 651 genes were upregulated and

enriched in biological pathways, including positive regulating of apoptosis (e.g., *Stk4* and *Bak1*) and mitogen-activated protein kinases (MAPK) cascade (e.g., *Ntrk2* and *Bcar3*). The significantly downregulated 1043 DEGs in sh*LncBAR* CMs were found to be associated with the cell cycle (e.g., *Mki67*, *Cdc20*, and *Ccnd2*), cell division (e.g., *Cdca2*, *Aurka*, and *Kif11*), and wound healing (e.g., *Postn* and *Col3a1*), consistent with our above findings (Fig. 6c).



We further performed Kyoto Encyclopedia of Genes and Genomes (KEGG) analysis and identified the enrichment of upregulated MAPK signaling and downregulated cell cycle pathway induced by sh*LncBAR* (Fig. 6d, e). Interestingly, pathways regulated by the SWI/SNF chromatin remodeling complex during cardiac lineage differentiation and myogenesis^{27,28}, including Wnt signaling pathway and EGFR tyrosine kinase

inhibitor resistance pathway, were significantly upregulated in sh*LncBAR* group (Fig. 6d). Further analysis revealed that the expression levels of several downstream factors (e.g., *Cdkn1a*, *Bmp10*, *Mcm6*, and *Cdc6*) reported to be regulated by BRG1 changed significantly after knockdown of *LncBAR* (Fig. 6f). These findings suggest that *LncBAR* can work synergistically with BRG1 to regulate cardiomyocyte proliferation and cardiac regeneration.

Fig. 5 | *LncBAR* promotes adult cardiomyocyte proliferation and heart repair post-MI. **a** Schematic of the experiment design for evaluating the role of *LncBAR* in adult mice post-MI. Adeno-associated virus serotype 9 (AAV9) with *LncBAR* overexpression driven by cardiac specific promoter cTnT (AAV9-cTnT-*LncBAR*) or control virus (AAV9-cTnT-Control) were intramyocardially injected into the injured site immediately following MI. Echocardiographic assessments were performed weekly. Heart samples were collected 2 weeks or 6 weeks post-MI. **b** Quantification of total cardiomyocyte number from hearts 2 weeks post-MI following *LncBAR* or control virus treatment ($n = 5$ mice). Hearts were perfused using a Langendorff apparatus, and isolated cardiomyocytes were counted using a hemocytometer. **c** Quantification of mononucleated, binucleated, and multinucleated cardiomyocytes isolated from hearts 2 weeks post-MI following *LncBAR* or control virus treatment. Hearts were perfused using a Langendorff apparatus, and isolated

cardiomyocytes were stained with α -actinin and DAPI for identification and nuclear counting. ($n = 5$ mice). Scale bars, 20 μ m. Representative confocal z-stack images and quantification of Aurora B+ cTnI+ CMs (**d**) Ki67+ cTnI+ CMs (**e**), and pH3+ cTnI+ CMs (**f**) in the border zones of mouse hearts 2 weeks post-MI. Yellow arrows indicate proliferating CMs ($n = 12$ fields, 3 mice/group). Scale bars, 20 μ m. Representative Masson's trichrome staining (**g**) of heart cross-sections and fibrotic area quantification (**h**) 6 weeks post-MI ($n = 5$ mice). Scale bars, 1 mm. Echocardiography analysis of mouse hearts. LVEF (**i**): left ventricular ejection fraction; LVFS (**j**): left ventricular fractional shortening ($n = 4$ mice for sham groups, $n = 8$ mice for MI groups, but 2 weeks post-MI $n = 5$ mice for MI groups). Data are presented as mean \pm SEM. Statistical significance was determined by two-tailed unpaired t test or two-way ANOVA with Tukey's multiple comparisons test. * $P < 0.05$, ** $P < 0.01$, *** $P < 0.001$.

The PI3K-AKT signaling plays crucial roles in the regulation of CM proliferation, survival and function^{29,30}. Our KEGG analysis indicated that *LncBAR* depletion reduced PI3K-AKT signaling (Fig. 6e). Western blot analysis confirmed elevated phosphorylation of PI3K and AKT in cardiomyocytes with *LncBAR* overexpression (Fig. 6g–i). Furthermore, treating *LncBAR* overexpressed NMCs with the AKT inhibitor LY294002 abrogated the pro-proliferative effect of *LncBAR* as evaluated by co-staining of cTnT with pH3 or Ki67 (Fig. 6j, k). Similarly, LY294002 treatment eliminated the effect of *LncBAR* on increasing the expression of cell cycle-related genes, including those involved in cell cycle initiation (*Ccnd1*, *Ccnd2*, and *Cdk6*), S phase and G2 phase progression (*Mcm3* and *Ccna2*), and the transition from metaphase to anaphase and the progression of anaphase (*Cdc20* and *Cdca2*) (Fig. 6l). Taken together, these data suggest that *LncBAR* exerts its functional role by activating the PI3K-AKT signaling pathway, thereby enhancing the proliferative capacity of cardiomyocytes. *LncBAR* promotes cardiomyocyte proliferation by stimulating PI3K-AKT pathway and subsequently enhancing the expression of downstream cell cycle genes.

Additionally, we noticed that sh*LncBAR* increased expression of apoptosis-related genes, which were also targets of PI3K-AKT pathway. RT-qPCR analyses confirmed that *LncBAR* knockdown increased the expression of pro-apoptotic genes, including *Bak1*, *Stk4*, *Moap1* and *Pidd1* (Supplementary Fig. 5a). We then challenged *LncBAR*-overexpressed NMCs and control NMCs with oxygen glucose deprivation and reperfusion (OGD/R)-induced apoptotic conditions, and assessed apoptotic cells with terminal deoxynucleotidyl transferase dUTP nick end labeling (TUNEL) staining. Our results showed that OGD/R treatment resulted in 20% cell death in control cells, whereas *LncBAR* overexpression reduced TUNEL+ NMCs to approximately 10% (Supplementary Fig. 5b). TUNEL staining of heart sections from AR mice also demonstrated significantly fewer TUNEL+ CMs in heart injected with AAV9-cTnT-*LncBAR* compared to controls (Supplementary Fig. 5c). These findings indicate that overexpression of *LncBAR* protects CMs from apoptosis under stressed conditions. We then intramyocardially injected AAV9-cTnT-*LncBAR* or control viruses into P1 *LncBAR* KO and WT mice. AR was performed at P8, and hearts were harvested 24 h post-surgery (AR1) for histological analyses (Supplementary Fig. 5d). TUNEL staining of heart sections revealed that *LncBAR* KO significantly increased TUNEL+ cardiomyocytes, while AAV9-mediated *LncBAR* supplementation attenuated this apoptotic response (Supplementary Fig. 5e). These findings are consistent with our RNA-seq analyses, which showed enrichment of GO pathways related to positive regulation of apoptosis in *LncBAR* deficient cardiomyocytes (Fig. 6c)

***LncBAR* directly binds to BRG1 and increases its protein abundance**

Our previous work demonstrated that *LncBAR* directly associates with the SWI/SNF complex in embryonic brain tissue²⁴, raising the possibility of a similar interaction in cardiomyocytes. Interestingly, *Brg1* expression significantly increased in the apical zone at AR7 compared to the border and remote zones, mirroring *LncBAR* expression (Fig. 7a).

To rigorously test whether *LncBAR* directly binds to BRG1 in cardiomyocytes, we performed RNA immunoprecipitation followed by

quantitative real-time PCR (RIP-qPCR) in HL-1 cardiomyocytes. Using three independent primer pairs (P1, P2 and P3) targeting different regions of *LncBAR*, RIP-qPCR consistently detected its enrichment in BRG1 immunoprecipitates compared to IgG controls (Supplementary Fig. 6a–c). These results revealed that *LncBAR* physically interacts with BRG1 in cardiomyocytes.

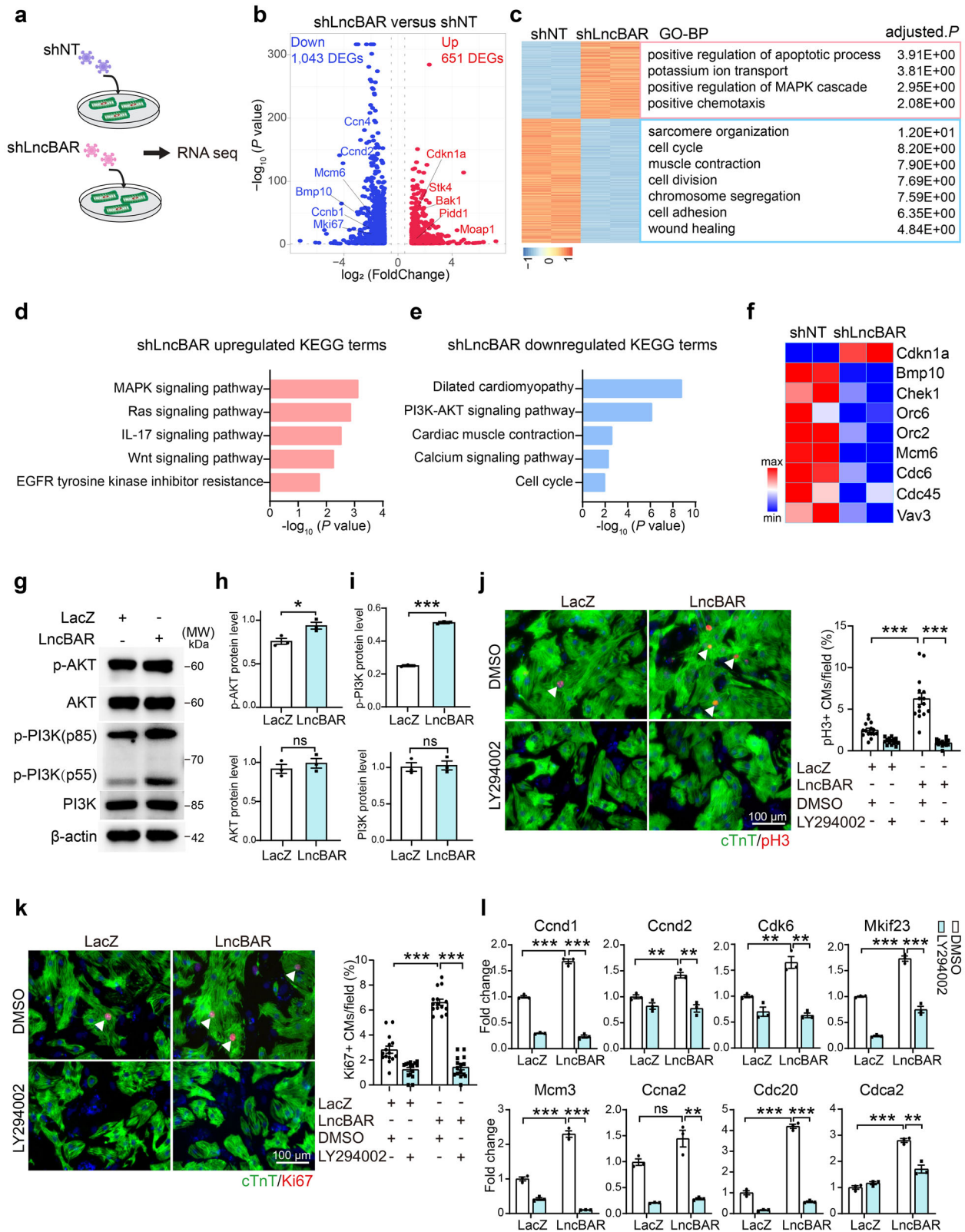
We next examined the effect of *LncBAR* on *Brg1* and found that neither knockdown nor overexpression of *LncBAR* affected *Brg1* expression at mRNA level (Fig. 7b). However, at the protein level, knockdown of *LncBAR* reduced BRG1 expression, whereas *LncBAR* overexpression elevated BRG1 levels (Fig. 7c, d). Additionally, expression of other components of the SWI/SNF chromatin remodeling complex, including BAF155 and BAF250a were consistently increased by *LncBAR* overexpression (Fig. 7d). These results suggest that *LncBAR* directly binds with BRG1 to regulate the SWI/SNF chromatin remodeling complex.

We next explored how *LncBAR* overexpression enhances BRG1 protein stability. Western blot analysis revealed that *LncBAR* overexpression significantly inhibited BRG1 degradation in NMCs following cycloheximide (CHX) treatment (Fig. 7e, f). Furthermore, the reduction in BRG1 protein levels caused by *LncBAR* knockdown was reversed by the proteasome inhibitor MG132, but not by the autophagosome inhibitor chloroquine (CQ) or the lysosome inhibitor NH₄Cl (Fig. 7g, h). Together, these findings indicate that *LncBAR* not only binds BRG1 but also stabilizes it by suppressing proteasome-mediated degradation.

***LncBAR* promotes cardiomyocyte proliferation through BRG1 in vitro**

Next, we investigated whether *LncBAR* induces cardiomyocyte proliferation through BRG1. We designed shRNAs targeting *Brg1*, achieving knockdown efficiency over 80%, and performed epistasis experiments (Fig. 7i). Lentiviral sh*Brg1* was introduced into NMCs with or without *LncBAR* overexpression, and the proliferation of treated NMCs were assayed by ICC with Ki67 and pH3. We found that while *LncBAR* overexpression consistently increased the number of Ki67+ and pH3+ NMCs, sh*Brg1* treatment significantly abrogated the *LncBAR*-induced NMC expansion (Fig. 7j, k).

We then assessed the expression levels of cell cycle-related genes across different phases (Fig. 7l), including *Cdk3* (G0/G1 and G1/S transition), *Mcm3*, *Ccnd1*, and *Ccnd2* (S phase initiation), *Cdca3* (G2/M transition), and *Ccnb1*, *Ccnb2*, and *Cdc20* (M phase progression). Knockdown of *Brg1* inhibited the upregulation of those cell cycle related genes in *LncBAR* overexpressing cardiomyocytes, suggesting that BRG1 is required for *LncBAR*-mediated cell cycle activation. Additionally, we analyzed published BRG1 ChIP-seq datasets³¹ and found the enrichment of BRG1 binding motifs located at the promoter regions of *MCM3* and *AURKA* (Fig. 7m, n), indicating its direct transcriptional regulation of these genes. Furthermore, the loss of *Brg1* reduced *LncBAR*-induced phosphorylation of PI3K and AKT, while their total protein levels remained largely unchanged (Fig. 7o–q). Collectively, these results suggest that *LncBAR* enhances cardiomyocyte proliferation through the upregulation of BRG1, which subsequently drives cell cycle progression.



LncBAR enhances cardiomyocyte proliferation and regeneration in vivo via BRG1

Building on our in vitro findings, we assessed BRG1 and PI3K-AKT activation in the apical zone at AR7 in LncBAR- or LacZ-treated animals. LncBAR overexpression increased BRG1 protein abundance and upregulated the expression of other SWI/SNF chromatin remodeling complex

components, including BAF155 and BAF250a (Fig. 8a, c). In parallel, LncBAR enhanced PI3K and AKT phosphorylation without affecting their total protein expression (Fig. 8a–e).

To determined how LncBAR-mediated BRG1 accumulation influences the cardiac regeneration, we generated four experimental groups through intramyocardial injection of saline or viral constructs for LncBAR

Fig. 6 | *LncBAR* overexpression positively regulated cardiomyocyte survival and proliferation. **a** Schematic depiction of experimental design using NMCs treated with sh*LncBAR* or shNT for RNA-seq ($n = 2$ biological replicates). **b** Volcano plot showing differentially expressed genes (DEGs) induced by *LncBAR* knockdown (sh*LncBAR*) in NMCs compared to those treated with shNT. DEGs were defined by $P < 0.05$ and $|\text{fold change}| \geq 2$ comparing sh*LncBAR*-NMCs to shNT-NMCs. **c** Gene Ontology (GO) analysis of significantly enriched pathways in sh*LncBAR*-treated NMCs compared with shNT-treated NMCs. Kyoto Encyclopedia of Genes and Genomes (KEGG) analysis showing significantly upregulated (**d**) and downregulated (**e**) pathways enriched in sh*LncBAR*-NMCs compared to shNT control cells. **f** Heatmap showing the expression levels of representative *Brg1* downstream factors involved in proliferation in sh*LncBAR*- or shNT-NMCs ($n = 2$ biological replicates). **g–i** Western blot showing the expression of total and

phosphorylated form of PI3K and AKT in NMCs treated with or without *LncBAR* overexpression. Quantification of indicated protein expression was shown in (**h**) and (**i**) ($n = 3$ biological replicates). Representative ICC images and quantification for cTnT+ pH3+ (**j**) and cTnT+ Ki67+ (**k**) NMCs treated with *LncBAR* along with small molecule LY294002 (PI3K/AKT pathway inhibitor). Cells infected with lentiviral LacZ and treated with DMSO were used as control. White arrows indicate proliferating NMCs ($n = 15$ fields). Scale bars, 100 μm . **l** RT-qPCR analysis showing expression of genes involved in positive regulation of cell cycle in *LncBAR* overexpressed NMCs treated with or without LY294002 inhibitor ($n = 3$ biological replicates). Data are presented as mean \pm SEM. Statistical significance was determined by two-tailed unpaired t test or two-way ANOVA with Tukey's multiple comparisons test. * $P < 0.05$, ** $P < 0.01$, *** $P < 0.001$.

overexpression and/or *Brg1* knockdown. AR injury was performed at non-regenerative stage (P8), and heart tissues were collected at AR7 and AR21 for histological and functional analyses (Fig. 8f). RT-qPCR confirmed *LncBAR* overexpression and *Brg1* knockdown (Fig. 8g). Immunofluorescence for cTnI with proliferation markers (Ki67 and pH3) revealed that *LncBAR* overexpression significantly increased proliferating cardiomyocytes at AR7 versus controls. Whereas, *Brg1* knockdown markedly attenuated this effect (Fig. 8h, i). By AR21, Masson's trichrome staining showed that *LncBAR* overexpression reduced fibrotic scarring, an effect abolished by *Brg1* depletion (Fig. 8j). Concomitantly, echocardiography demonstrated that the functional improvements of *LncBAR*, as indicated by increased LVEF/LVFS and reduced LVEDV/LVESV were lost upon *Brg1* knockdown (Fig. 8k–n). Together, these results confirmed that BRG1 mediates *LncBAR*-induced cardiomyocyte proliferation and cardiac regeneration following AR.

***LncBAR* overexpression promotes the proliferation and survival of human embryonic stem cell-derived cardiomyocytes**

Although we did not identify a conserved sequence of *LncBAR* in humans²⁴, we asked whether the identified *LncBAR* sequence could still promote human cardiomyocyte proliferation. We used human embryonic stem cell-derived cardiomyocytes (hESC-CMs) at day 10 of differentiation, which exhibited spontaneous beating (Supplementary Movie 1) and reached approximately 70% purity (Supplementary Fig. 7a, b). ICC analyses indicated that most cells were immature, with ~60% showing disorganized and ~10% well-aligned sarcomere structures, making them suitable for studying proliferation (Supplementary Fig. 7c).

We next determined a transduction efficiency of approximately 97% for our lentiviral vectors in hESC-CMs and RT-qPCR confirmed *LncBAR* overexpression (Supplementary Fig. 7d and Fig. 9a). ICC for cTnT and Ki67 or cTnT and Aurora B showed a significantly two-fold increase in the percentage of proliferating hESC-CMs with *LncBAR* overexpression (Fig. 9b, c). Consistently, the number of EdU+ and pH3+ hESC-CMs were doubled in *LncBAR* overexpressed CMs compared to controls (Supplementary Fig. 7e, f). Furthermore, to directly demonstrate cardiomyocyte proliferation, we quantified the number of hESC-CMs following *LncBAR* overexpression, showing a significant increase consistent with enhanced cell division (Supplementary Fig. 7g).

At the transcriptional level, RT-qPCR analysis showed that overexpression of *LncBAR* triggered the significant increase of a panel of genes positively regulating cell cycle, including control of mitosis and G1 phase progression (*CDC16*), initiation of S phase (e.g., *CDK2*, *CDK4*, *CCND2*, and *CCNE2*), promotion of G2 to M phase transition (*CDK1* and *CHEK1*), and M phase progression (*CCNB1* and *CCNB2*) (Fig. 9d). Conversely, negative regulators of the cell cycle, including *p27* and *p16*, which switch off *CDK2*, 4 and 6 and arrest the cell cycle, demonstrated reduced expression in *LncBAR*-transduced hESC-CMs compared to control cells (Fig. 9e). These findings indicate that *LncBAR* enhances the hESC-CM proliferation by modulating the expression of both positive and negative cell cycle regulators.

We next assessed whether *LncBAR* exerts its effects on hESC-CM proliferation through BRG1. Western blot analysis showed that *LncBAR* overexpression significantly inhibited BRG1 degradation in CHX-treated

human cardiomyocytes (Supplementary Fig. 7h), consistent with its role in murine cardiomyocytes. We then designed shRNAs targeting *BRG1* achieving efficient knockdown (Fig. 9f). As expected, loss of *BRG1* in hESC-CMs abolished the enhanced cell proliferation induced by *LncBAR*, as determined by pH3 and cTnT staining (Fig. 9g). At the protein level, introducing sh*BRG1* into hESC-CMs with *LncBAR* overexpression reduced the phosphorylation of PI3K and AKT, while having minor effects on total protein expression (Fig. 9h–j). Together, these results indicate *LncBAR* interacts with BRG1 to activate the cell cycle progression, promoting hESC-CM proliferation.

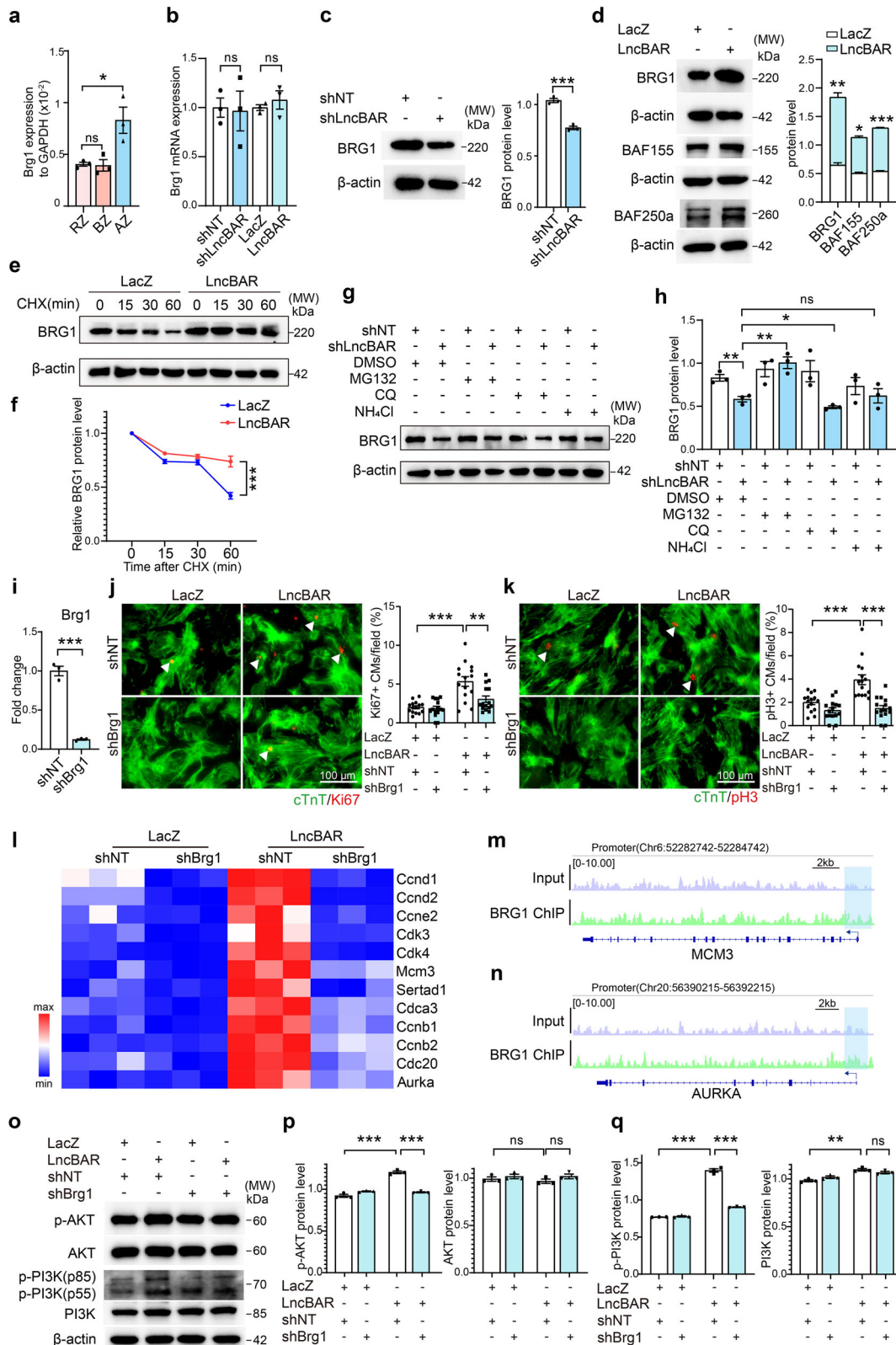
In addition to its pro-proliferative role, we examined whether *LncBAR* also enhances hESC-CMs survival under stress conditions. We performed TUNEL staining with *LncBAR*-transduced cells upon OGD/R treatment. CMs transduced with LacZ virus were used as controls. We found that *LncBAR* overexpression significantly reduced apoptosis, lowering the percentage of TUNEL+ cells from approximately 30% in controls to around 12% (Fig. 9k). Congruently, ICC for cleaved caspase3 (casp3) further confirmed that *LncBAR* overexpression reduced the number of apoptotic cells (Fig. 9l). Additionally, western blot analysis showed that overexpression of *LncBAR* reduced the protein expression of casp3 (Fig. 9m).

Together, our results demonstrated that although *LncBAR* lacks a conserved human sequence, its expression in hESC-CMs is still capable of enhancing cardiomyocyte proliferation. This suggests that while a direct human homolog of *LncBAR* has not been identified, functionally analogous regulatory elements or short sequence motifs may exist in the human genome, enabling similar effects on cardiomyocyte proliferation.

Discussion

In this study, we identified *LncBAR*, a novel lncRNA that regulates cardiomyocyte proliferation and heart regeneration. We demonstrated that *LncBAR* deficiency impaired heart regeneration, whereas its overexpression promoted cardiomyocyte proliferation and improved post-AR cardiac function. Furthermore, *LncBAR* overexpression promoted adult cardiomyocyte proliferation and enhanced heart repair following myocardial infarction. Mechanistically, *LncBAR* directly interacts with BRG1 and upregulates its protein expression, which in turn activates cell cycle progression. These findings underscore the pivotal roles of *LncBAR*-BRG1 connection in cardiac regeneration, offering a novel strategy to enhance cardiac repair.

lncRNAs are crucial regulators of cardiac development, differentiation and diseases, with their expression tightly associated with developmental and stress conditions in the heart^{32,33}. Our work demonstrated that *LncBAR* expression declines from embryonic (E13.5) to adult stages (12 weeks old), suggesting its potential role in heart regeneration. Functional analysis confirmed that *LncBAR* actively stimulates cardiomyocyte proliferation and improves cardiac function after injury. These results established *LncBAR* as a positive regulator for cardiomyocyte renewal, supporting the notion that developmental correlated lncRNAs could be reactivated to enhance cardiac repair in the adult heart. Recent studies have shown that lncRNA *CPR* (cardiomyocyte proliferation regulator) represses CM proliferation, while lncRNA *Snhg1* (small nucleolar RNA host gene 1) promotes it^{25,34}. These



observations, along with our research, reinforce the critical role of LncRNAs in cardiac repair, suggesting a complex regulatory network controlling cardiomyocyte proliferation and regeneration.

Brg1, the core component of the SWI/SNF ATP-dependent chromatin-remodeling complex also known as SWI/SNF-related matrix-associated actin-dependent regulator of chromatin subfamily A member 4 (*Smarca4*),

has been recognized as a crucial regulator of cardiomyocyte proliferation. In zebrafish heart, depletion of *Brg1* upregulates *Cdkn1a* and *Cdkn1c* expression after AR and inhibits myocardial regeneration¹⁶. In mammalian embryonic and postnatal heart, knockdown of *Brg1* decreases expression level of *Bmp10* while increased expression level of *Cdkn1c*^{14,35}, thereby inhibiting cardiomyocyte growth. Our study identified a previously

Fig. 7 | *LncBAR* facilitates cardiomyocyte proliferation by upregulating BRG1 protein levels. **a** RT-qPCR analysis of *Brg1* expression in AR7 hearts. RZ remote zone, BZ border zone, AZ apex zone ($n = 3$ mice). **b** RT-qPCR analysis of *Brg1* expression (relative to GAPDH) in NMCs following *LncBAR* knockdown or overexpression, with shNT or LacZ as controls respectively ($n = 3$ biological replicates). **c** Western blot and quantification of BRG1 protein levels in NMCs treated with or without sh*LncBAR* ($n = 3$ biological replicates). **d** Western blot and quantification of BRG1, BAF155 and BAF250a in NMCs upon *LncBAR* overexpression, with LacZ as control ($n = 3$ biological replicates). Western blot analysis (**e**) and quantification (**f**) of BRG1 expression in *LncBAR*-overexpressing NMCs treated with cycloheximide (CHX, 10 $\mu\text{g}/\text{ml}$) for indicated times ($n = 3$ biological replicates). Western blot analysis (**g**) and quantification (**h**) of BRG1 expression in *LncBAR*-depleted NMCs treated with proteasome inhibitor MG132 (10 μM), or lysosomal inhibitors chloroquine (CQ, 10 μM) and NH_4Cl (25 mM) for 6 h ($n = 3$

biological replicates). **i** RT-qPCR analysis of *Brg1* expression in sh*Brg1*-transduced NMCs, with shNT as control ($n = 3$ biological replicates). Representative ICC and quantification of cTnT+ Ki67+ (**j**) and cTnT+ pH3+ (**k**) cells in NMCs overexpressing *LncBAR*, treated with either sh*Brg1* or shNT control. White arrows indicate proliferating NMCs ($n = 15$ fields). Scale bars, 100 μm . **l** RT-qPCR analysis of cell cycle genes in *LncBAR*-overexpressing NMCs treated with sh*Brg1* or shNT lentiviruses ($n = 3$ biological replicates). ChIP-seq profiling showed the binding signal for BRG1 at the genomic loci of *MCM3* (**m**) and *AURKA* (**n**) promoter regions in reported Nalm-6 cell line³¹. Western blot (**o**) and quantification (**p**, **q**) of total and phosphorylated PI3K and AKT in NMCs with *LncBAR* overexpression and *Brg1* knockdown ($n = 3$ biological replicates). Data are presented as mean \pm SEM. Statistical significance was determined by two-tailed unpaired *t* test, one-way ANOVA, or two-way ANOVA with Tukey's multiple comparisons test. * $P < 0.05$, ** $P < 0.01$, *** $P < 0.001$.

unrecognized mechanism by which *LncBAR* regulates BRG1 at the post-transcriptional level. Specifically, *LncBAR* enhances BRG1 protein stability without altering its mRNA expression, thereby sustaining BRG1 activity to drive cardiomyocyte cell-cycle progression. Nonetheless, the precise molecular mechanism, such as the involvement of the ubiquitin-proteasome pathway, warrants further investigation.

Although *LncBAR* itself lacks overt sequence conservation in humans, it retains the capacity to promote proliferation of human cardiomyocytes. This observation raises the possibility that functionally analogous lncRNAs or conserved regulatory motifs may exist across species to mediate similar effects. Importantly, BRG1 is highly conserved between mouse and human, sharing 97.2% protein identity, and serves as a critical epigenetic regulator in both species¹⁴. Such conservation suggests that mouse *LncBAR* may also interact with human BRG1 and activate similar downstream pathways, offering a mechanistic basis for its cross-species activity.

Interestingly, previous studies have revealed that *Brg1* mediates cardiac pressure overload-induced myocardial hypertrophy through at least two mechanisms. First, *Brg1* interacts with HDAC and PARP to repress α -MHC while activating β -MHC expression¹⁴. Second, *Brg1* binds with *Mhrt779* to inhibit HDAC2/p-AKT/p-GSK3 β pathway, thereby exerting an anti-hypertrophic effect³⁶. In line with these findings, our study revealed that *LncBAR* loss reduces BRG1 expression and cardiomyocyte size, suggesting a potential link between *LncBAR*, BRG1, and myocardial hypertrophy. Further investigations are needed to unravel the intricate relationship between these factors and their role in cardiac remodeling.

The PI3K-AKT pathway has been widely reported to promote cardiomyocyte proliferation during development and neonatal stages, and its reactivation in adult or injured hearts can stimulate limited CM proliferation and regeneration^{34,37,38}. Consistently, this pathway is commonly activated in proliferating cardiomyocytes^{26,39}. Upstream signaling pathways, such as Hippo-Yap signaling, cell surface tyrosine kinases ErbB2, ErbB4 and IGFR, act through PI3K-AKT to effectively stimulate CM proliferation^{37,40,41}. In our research, we found that *LncBAR* overexpression activates PI3K-AKT signaling, whereas pharmacological inhibition of this pathway blocks *LncBAR*-induced cardiomyocyte expansion. However, the precise mechanism by which PI3K-AKT becomes activated remains elusive. One possibility is that BRG1, stabilized by *LncBAR*, drives the expression of key cell cycle regulators that in turn engage PI3K-AKT signaling. Alternatively, BRG1 and PI3K-AKT may represent parallel yet converging downstream pathways of *LncBAR*, both contributing to the proliferative response. Future studies, particularly comprehensive proteomic analyses, will be essential to dissect the interplay between these pathways and to define the signaling hierarchy underlying *LncBAR*-mediated cardiac regeneration.

While our study established *LncBAR* as a positive regulator of cardiomyocyte proliferation and cardiac repair, several limitations should be acknowledged. In this study, we used systemic *LncBAR* knockout mice and intramyocardial injection of sh*LncBAR* lentivirus to assess the effect of *LncBAR* deficiency on cardiac regeneration. Although our data indicated that *LncBAR* is preferentially expressed in cardiomyocytes and exerts

minimal effects on fibroblasts and endothelial cells under homeostatic conditions, we cannot fully exclude contributions from other cell types or potential combinatory effects within the tissue microenvironment. Further work using cardiomyocyte-specific *LncBAR* deficient genetic models will be helpful. In addition, we observed increased fibrosis in *LncBAR* KO hearts following apical resection, but the underlying mechanisms by which *LncBAR* regulates fibrosis remain to be determined.

To evaluate CM proliferation, we applied multiple complementary approaches, including immunostaining for canonical markers (pH3, Ki67 and Aurora B kinase) and cardiomyocyte number quantification following the guideline⁴². Nonetheless, additional methods, including single-cell transcriptomic analyses to distinguish subpopulation of CMs at different cell cycle states, and advanced genetic models such as the mosaic analysis with double markers (MADM) mouse⁴³, would provide more rigorous validation and deeper mechanistic insights.

Overall, our results elucidate a critical *LncBAR*-BRG1 axis in promoting cardiomyocyte proliferation and efficient cardiac repair. We revealed that overexpression of *LncBAR* promoted cardiomyocyte proliferation in both murine and human cardiomyocytes, offering new insights into lncRNA-mediated cardiac regeneration. These findings provide an important insight for future studies exploring lncRNA-based therapeutic strategies for heart repair and regeneration.

Methods

Mouse strains and ethical approval

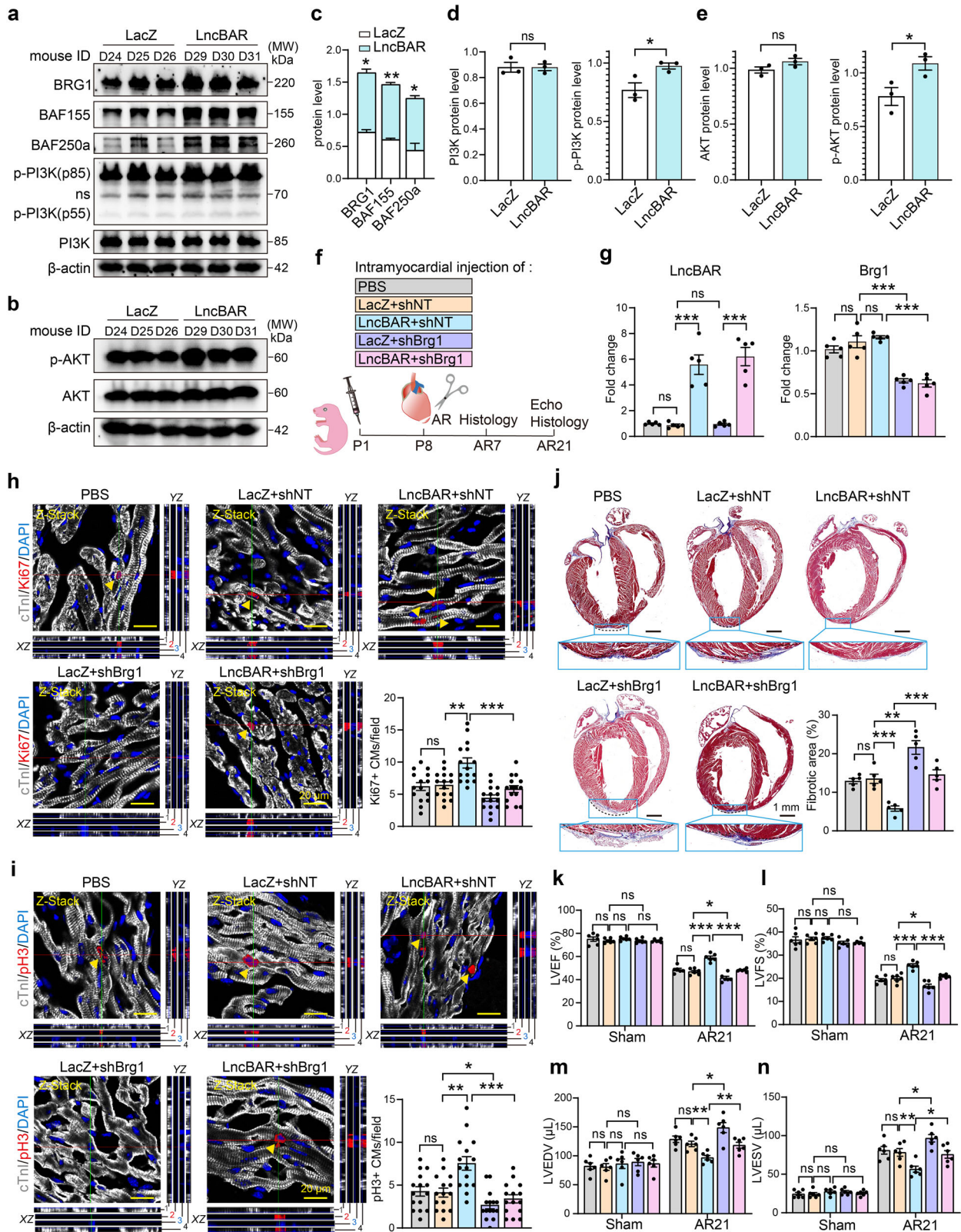
All mice were maintained in specific pathogen-free (SPF) facilities at the Medical Research Institute of Wuhan University. The experimental protocols followed the International Guiding Principles for Biomedical Research Involving Animals. All animal experiments were approved by the Animal Care and Ethical Committee of Medical Research Institute at Wuhan University (approval number: MRI2020-LAC68), and conform to the National Institutes of Health (NIH) Guidelines for the Care and Use of Laboratory Animals. Both male and female mice were used in this study. Wild-type C57BL/6 and CD1 mice were obtained from the Beijing Vitalstar Biotechnology Co., Ltd. (Beijing, China). The *LncBAR*^{-/-} mice were generated and maintained as previously described²⁴. The genotyping primers were listed in Supplementary Table 1.

Plasmid construction

For gene overexpression, pLenti-*LncBAR* was cloned into lentiviral backbone that was originally purchased from Addgene (#17448). The construct pLenti-LacZ was used as control. All shRNAs were annealed in the pLKO.1 backbone as previously described⁴⁴. All cloning primers were listed in Supplementary Table 1, and all constructs were confirmed by sequencing.

Cell culture and viral production

HEK293T cells were purchased from ATCC and cultured in Dulbecco's modified Minimal Essential Medium (DMEM) (Gibco, 6123110) supplemented with 10% fetal bovine serum (FBS) (Newzerum, FBS-AU500), 1%



penicillin/streptomycin (Hyclone, SV30010), and 1% non-essential amino acids (NEAA) (Gibco, 1114050). Viral package was performed as previously defined^{44,45}. Briefly, 293T cells were transfected with 10 μ g viral constructs, 7 μ g psPAX2 and 3 μ g pMD2.G using Polyethylenimine (PEI) (Polysciences, 24765). The supernatant was collected 48 h and 72 h after transfection, filtered through 0.45 μ m filter (Merck Millipore), and incubated

with PEG6000 solution (8% final concentration) overnight at 4 $^{\circ}$ C. Then the mixture was spun down at 3800 rpm for 30 min at 4 $^{\circ}$ C, and the pelleted virus was resuspended with 100 μ L of DMEM medium per each 10 cm dish. Lentivirus can be used in fresh or frozen at -80 $^{\circ}$ C.

To prepare the lentivirus for in vivo experiments, the virus-containing supernatant was filtered through 0.45 μ m filter, and concentrated by

Fig. 8 | *LncBAR* enhances cardiomyocyte proliferation and cardiac regeneration by activating BRG1 and PI3K-AKT pathway. Western blot analysis and quantification of the SWI/SNF complex subunits (a, c) and PI3K-AKT pathway activation (a, b, d, e) in apical tissue post-AR injury ($n = 3$ biological replicates). f Schematic depiction of AR experiments. Viruses harboring *LncBAR*, *shBrg1*, or respective controls were intramyocardially injected into neonatal mouse hearts, with PBS as a non-viral control. AR surgery was performed at P8. Echocardiography and histological samples were collected at AR7 and AR21. g RT-qPCR analysis showing the expression level of *LncBAR* and *Brg1* in hearts receiving the virus injection ($n = 5$ mice). Representative confocal z-stack images and quantification of Ki67+ cTnI+

CMs (h), and pH3+ cTnI+ CMs (i) in apex zone of AR7 hearts. Yellow arrows indicate Ki67+ or pH3+ CMs ($n = 15$ fields, 3 mice/group). Scale bars, 20 μ m. j Representative Masson's trichrome-stained sagittal heart sections with fibrotic area quantification at AR21 ($n = 5$ mice). Scale bars, 1 mm. Echocardiography analysis of mouse hearts at AR21. LVEF (k): left ventricular ejection fraction; LVFS (l): left ventricular fractional shortening; LVEDV (m): left ventricular end-diastolic volume; LVESV (n): left ventricular end-systolic volume ($n = 6$ mice). Data are presented as mean \pm SEM. Statistical significance was determined by two-tailed unpaired t test, one-way ANOVA, or two-way ANOVA with Tukey's multiple comparisons test. * $P < 0.05$, ** $P < 0.01$, *** $P < 0.001$.

ultracentrifugation at 23,000 rpm for 1 h and 45 min. The pelleted virus was resuspended with DPBS and polybrene (8 μ g/mL, Merck Millipore). 10 μ L of virus mixture was injected into the cardiac ventricles using an insulin syringe equipped with a 30-gauge needle.

Isolation and culture of primary neonatal mouse cardiomyocytes (NMCMs)

Neonatal mice (1–3 days old) were subjected to decapitation and the hearts were extracted and rinsed with ice-cold PBS for three times. CMs were then dissociated using Neonatal Heart Dissociation kit (Miltenyi Biotec, 130-098-373) following manufacturer's instructions. Briefly, the ventricles were minced into small pieces and digested with enzymes from the reagent kit at 37 °C for 15 min. Tissues were dissociated with gentleMACS™ Dissociator (Miltenyi Biotec, 130-093-235) into single-cell suspensions. The supernatant was filtered through 100 μ m cell strainers (Nest, 258367) and cells were collected by centrifuge at 1000 rpm for 5 min. Red blood cells were removed using red blood cell lysis buffer (0.15 M NH₄Cl, 0.1 M Na₂EDTA-2H₂O, 10 mM KHCO₃). The remaining cells were washed with MACS buffer (DPBS with 2% FBS and 0.1 mM EDTA) and incubated with antibodies provided in the Neonatal Cardiomyocyte Isolation Cocktail kit (Miltenyi Biotec, 130-100-825) for 15 min at 4 °C. After two rounds of wash with MACS buffer, cells were applied to MACS buffer-calibrated LS column (Miltenyi Biotec, 130-042-401) and the flow-through containing unlabeled CMs was collected for use.

Isolation of adult murine cardiomyocytes

WT and *LncBAR* KO mice hearts were perfused with Langendorff apparatus as described with minor modification⁴⁶. Briefly, mice were anesthetized by intraperitoneal injection of a mixture of tribromoethanol (320 mg/kg) and 2-butanol (160 mg/kg) and were euthanized using cervical dislocation. Hearts were extracted and retrograde perfusion was immediately performed through an aortic cannulation with continuous flow at the speed of 16–24 drops/min in a Langendorff apparatus. Both ventricles were digested with 1 mg/mL collagenase II (Worthington, LS004176) for 10–15 min, followed by further mechanical dissociation with pipetting. The cell suspension was collected and filtered through a 100 μ m cell strainer. Cardiomyocytes were then collected for subsequent experiments.

Isolation of primary neonatal mouse cardiac fibroblasts (CFs)

To obtain neonatal CFs, hearts from neonatal mice (P1 to P3) were harvested and washed with PBS to remove blood cells. Then, clean hearts were minced roughly and transferred to 10 mL warm trypsin-EDTA (Sigma, T3924), and incubated at 37 °C for 10 min. The supernatant was discarded and the heart pieces were digested with 10 mL collagenase type II (Worthington, LS004176) for 8 min at 37 °C, followed by gentle vortex for 1 min. The supernatant was collected and diluted with 5 mL FB medium. After five rounds of collagenase digestion and collection.

Cell suspension was obtained by passing through 40 μ m cell strainer. Cell pellet was collected and CFs were sorted by magnetic activated cell sorting (MACS) as described previously⁴⁷. Cells were incubated with biotin anti-Thy1.2 antibody (Invitrogen, 13-0903-85) for 30 min at 4 °C, followed by anti-Biotin Microbeads (Miltenyi Biotec, 130090485) for 30 min at 4 °C. The cells were then washed and resuspended in MACS buffer (DPBS with

0.5% BSA and 2 mM EDTA) and applied to calibrated LS columns (Miltenyi Biotec, 130042401). Cells that bound beads were flushed out after three washes and ready to seed for experiments.

Isolation of primary neonatal mouse cardiac endothelial cells (ECs)

Neonatal mouse cardiac endothelial cells were isolated following established protocols⁴⁸. Briefly, hearts from neonatal mice (P1–P3) were harvested and washed with PBS to remove blood cells. Then hearts were cut with scalpel blade into small pieces and transferred to 5 mL heart digestion buffer (DMEM with 0.1% collagenase II and 0.25% collagenase IV and 7.5 μ g/mL DNase I) and incubated at 37 °C for 25 min. The mix were dissociated with gentleMACS™ Dissociator (Miltenyi Biotec, 130-093-235) into single-cell suspensions. The supernatant was filtered through 100 μ m cell strainers (Nest, 258367) and cells were collected by centrifuge at 300 \times g for 7 min. Resuspend the pellet and filter through a 40 μ m cell strainer. Centrifuge at 300 \times g for 5 min, remove the supernatant. Cell pellet was collected and ECs were sorted by magnetic activated cell sorting (MACS). Cells were incubated with biotin anti-CD31 antibody (Invitrogen, 13-0311-82) for 30 min at 4 °C, followed by anti-Biotin Microbeads (Miltenyi Biotec, 130090485) for 30 min at 4 °C. The cells were then washed and resuspended in MACS buffer (DPBS with 0.5% BSA and 2 mM EDTA) and applied to calibrated LS columns (Miltenyi Biotec, 130042401). Cells that bound beads were flushed out after three washes and ready to seed for experiments.

Human embryonic stem cell-derived CMs (hESC-CMs)

The human H7 ESC line was originally purchased from WiCell and was kindly gifted from Dr. Ning Sun's lab at Fudan University⁴⁹. The cell line was maintained and differentiated to hESC-CMs using well established protocol as previously reported⁵⁰. Differentiated beating hESC-CMs were digested and reseeded onto plates coated with Matrigel (Corning, 354277) for further research.

Oxygen–glucose deprivation and reperfusion (OGD/R) treatment

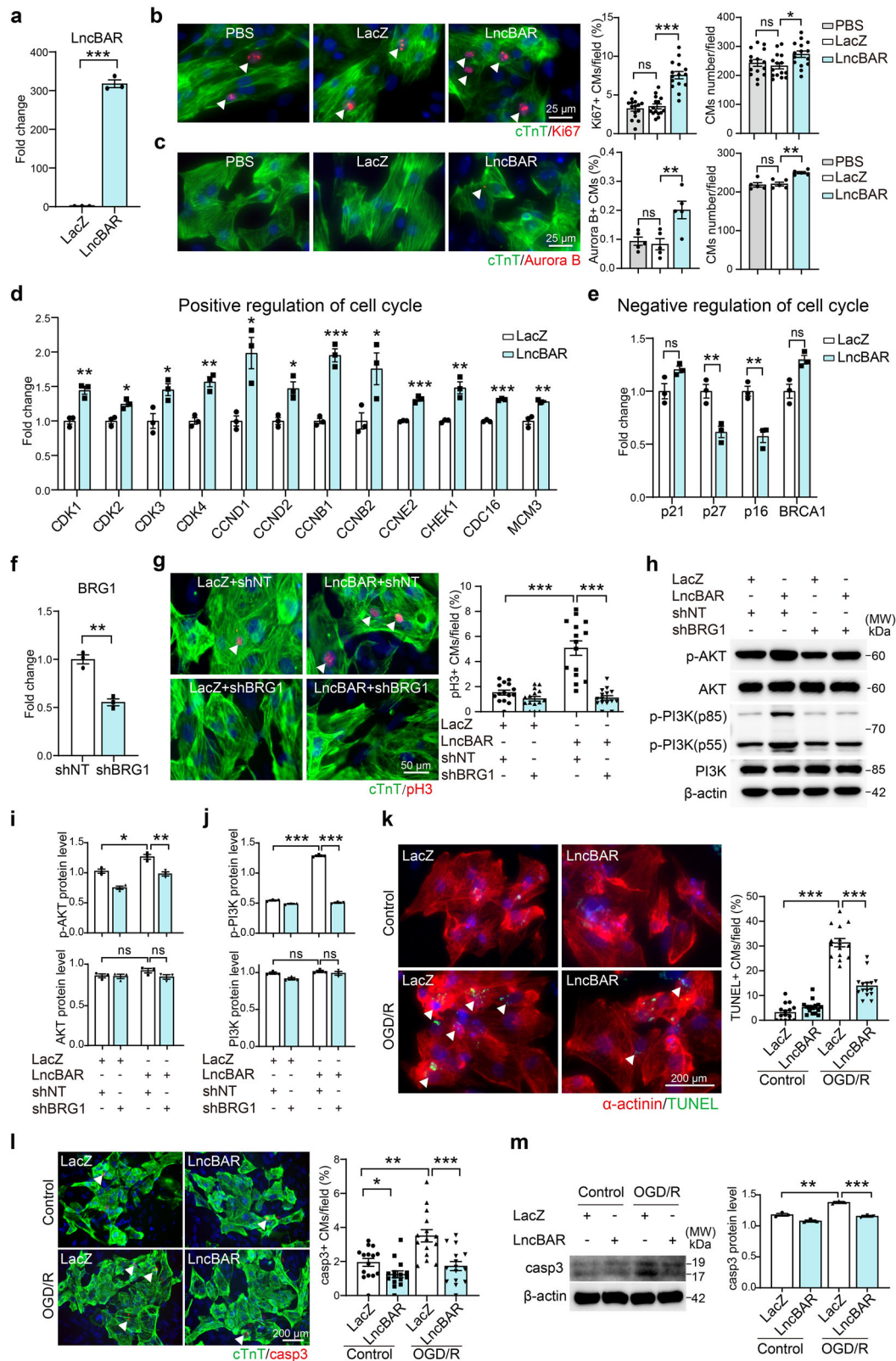
The OGD/R treatment was performed as previously described⁵¹. Briefly, NMCMs and hESC-CMs were incubated in glucose-free DMEM medium (Gibco, 2323743) within an anaerobic chamber (1% O₂, 5% CO₂) at 37 °C for 10 h to achieve oxygen-glucose deprivation (OGD). The cells were then transferred to normoxic conditions (95% air, 5% CO₂) and cultured with normal culture medium for 24 h at 37 °C (reperfusion, R). Control cells are treated the same medium but without OGD/R challenge.

5-ethynyl-20-deoxyuridine (EdU) incorporation assay

EdU labeling was carried out by culturing cells with 10 μ M EdU for 48 h before fixation. Cells were then stained using the Cell-Light EdU Apollo567 In Vitro Kit (Ribobio, C10310-1) according to manufacturer's instruction. Nuclei staining was performed with DAPI. Images were captured using Nikon Eclipse Ti2 fluorescence microscope.

Terminal deoxynucleotidyl transferase-mediated dUTP Nick End Labeling (TUNEL) assay

Cell apoptosis was evaluated using the One-step TUNEL In Situ Apoptosis Kit (Elabscience, AK15560) following manufacturer's instructions. Briefly,



tissue sections or cultured cells were fixed in 4% PFA for 15 min and subsequently permeabilized with 0.2% Triton X-100 for 10 min at 37 °C. Samples were then incubated with the TUNEL label reaction solution for 60 min at 37 °C. Images were acquired using Leica Thunder microscope (for tissue sections) and Nikon Eclipse Ti2 fluorescence microscope (for cultured cells).

Western blots

Cells or heart tissue were lysed by using protein lysis buffer (50 mM Tris-HCl pH 7.4, 150 mM NaCl, 1% NP40, 1 mM EDTA) with a complete phosphatase and protease inhibitor cocktail. The antibodies used in this assay were listed in Supplementary Table 2. Unprocessed original scans of western blots were deposited in Supplementary Fig. 8.

Fig. 9 | *LncBAR* overexpression improves proliferation and survival of human embryonic stem cell-derived cardiomyocytes (hESC-CMs). **a** RT-qPCR detecting *LncBAR* expression in hESC-CMs transduced with *LncBAR*- or control (LacZ)-encoding lentivirus ($n = 3$ biological replicates). **b** Representative ICC and quantification of cTnT+ Ki67+ hESC-CMs with *LncBAR* overexpression versus LacZ or PBS controls. White arrows indicate proliferating hESC-CMs ($n = 15$ fields). Scale bars, 25 μm . **c** Representative ICC and quantification of cTnT+ Aurora B+ hESC-CMs with *LncBAR* overexpression versus LacZ or PBS controls. White arrows indicate proliferating hESC-CMs. ($n = 5$ biological replicates). Scale bars, 25 μm . **d** RT-qPCR detecting the expression of genes promoting (**d**) and inhibiting (**e**) cell cycle progression in *LncBAR*-overexpressing hESC-CMs vs. LacZ control ($n = 3$ biological replicates). **f** RT-qPCR analysis of *BRG1* expression in hESC-CMs transduced with sh*BRG1* lentivirus ($n = 3$ biological replicates). **g** Representative ICC and quantification of cTnT+ pH3+ hESC-CMs treated with *LncBAR*-overexpressing together with sh*BRG1* or shNT control. White arrows indicate

proliferating hESC-CMs ($n = 15$ fields). Scale bars, 50 μm . Western blot (**h**) and quantification (**i, j**) of total and phosphorylated PI3K and AKT in hESC-CMs with *LncBAR* overexpression and sh*BRG1* knockdown ($n = 3$ biological replicates). **k** Representative ICC and quantification of apoptotic hESC-CMs with *LncBAR* overexpression. hESC-CMs with or without *LncBAR* overexpression were subjected to α -actinin and TUNEL staining under normal or oxygen-glucose deprivation/reperfusion (OGD/R) conditions. White arrows indicate TUNEL+ hESC-CMs ($n = 15$ fields). Scale bars, 200 μm . **l** Representative ICC and quantification of hESC-CMs probed with cleaved caspase 3 (casp3) and cTnT. Cells were treated as in (**k**). White arrows indicate casp3+ hESC-CMs ($n = 15$ fields). Scale bars, 200 μm . **m** Western blot showing the protein level of cleaved caspase 3 in *LncBAR*-overexpressing hESC-CMs subjected to OGD/R treatment ($n = 3$ biological replicates). Data are presented as mean \pm SEM. Statistical significance was determined by two-tailed unpaired *t* test, one-way ANOVA, or two-way ANOVA with Tukey's multiple comparisons test. * $P < 0.05$, ** $P < 0.01$, *** $P < 0.001$.

Immunofluorescence staining (ICC)

For ICC, cells were washed three times with PBS and fixed by 4% paraformaldehyde (PFA) for 15 min at room temperature. Next, cells were permeabilized with 0.1% Triton X-100, and blocked with 5% BSA for 1 h. Treated cells were incubated with primary antibodies listed in Supplementary Table 2 in 1% BSA overnight. After washing with PBS three times, cells were incubated with secondary antibodies for 1 h in dark. Nuclei staining was performed with DAPI. Around 20 images were randomly taken under $\times 10$ or $\times 20$ magnification at the same exposure setting for quantitative analyses.

RT-qPCR

Total RNA was extracted from cells or heart tissue by Trizol reagent (TaKara, 9109) and reverse-transcribed into cDNA using 5 \times HiScript IIRT SuperMix for qPCR (Vazyme, R222-01). RT-qPCR was performed using qPCR SYBR Green Master Mix (Yeastar, 11201ES08) on the Bio-Rad Real-Time PCR Detection System. Primer sequences used in present study were provided in Supplementary Table 3. The relative expression level was qualified using the $2^{-\Delta\Delta Ct}$ method.

Wheat germ agglutinin (WGA) staining

WGA (Invitrogen, W32464) staining was performed to assess cardiomyocytes hypertrophy. Briefly, heart sections were washed three times with HBSS (Gibco, C14175500BT). Then treated sections were incubated with WGA conjugated to Alexa Fluor 555 for 1 h at room temperature and then washed with HBSS. The cross-sectional cell size was measured by Image J software. At least 30 fields and 90 cells were randomly analyzed for each group.

RNA Immunoprecipitation qPCR (RIP- qPCR)

To obtain sufficient cardiomyocytes for RIP-qPCR experiments, we employed HL-1 cells, an immortalized mouse cardiomyocyte line that can be continuously expanded while retaining essential cardiomyocyte characteristics. HL-1 cells were subjected to ultraviolet (UV) crosslinking at 254 nm with an energy of 400 MJ/cm². And then cells were homogenized in ice-cold lysis buffer (50 mM Tris-HCl pH 7.4, 150 mM NaCl, 1% NP-40, 1 mM EDTA, 1:100 protease inhibitors cocktail, 1:25 RNase inhibitor). After incubating on ice for 10 min to lysis the cell, the lysate was centrifuged at 12,000 $\times g$ for 15 min at 4 $^{\circ}\text{C}$. The 5% lysis sample was stored for "input", and the remaining was used in immunoprecipitation reactions with an anti-Flag antibody and mouse IgG, respectively. The RNA of input and RIP was extracted using Trizol reagent (TaKara, 9109). RT-qPCR was performed using qPCR SYBR Green Master Mix (Yeastar, 11201ES08) on the Bio-Rad Real-Time PCR Detection System. Primer sequences were provided in Supplementary Table 3.

Flow cytometry

Cells were harvested by trypsin digestion at 37 $^{\circ}\text{C}$ for 3 min and fixed and permeabilized by fixation buffer (Biolegend, 420801), then incubated with

antibodies listed in Supplementary Table 2 at RT for 30 min at concentrations recommended by manufacturers. Cells were then suspended with 1% PFA and run with BD flow cytometer. FlowJo v10 was used to analyze the flow cytometry data.

Cell cycle analysis

To analyze the cell cycle profile, cell pellets from the HL-1 cells were fixed in 2 mL of ice-cold 70% ethanol overnight at -20 $^{\circ}\text{C}$. Fixed cells were collected by centrifugation and stained with 200 μL of propidium iodide (PI)/RNase staining solution (Invitrogen, F10797) for 20 min at room temperature in the dark. Stained cells were then examined by BD flow cytometer and FlowJo v10 was used to analyze the cell cycle profile.

Bulk RNA sequencing (RNA-seq) and analysis

In general, 2×10^5 CMs infected with sh*LncBAR* or shNT lentiviruses were collected in Trizol (Takara) for RNA extraction. RNA quality was assessed by examining A260/A280 ratio with NanodropTM OneCspectrophotometer (Thermo Fisher Scientific Inc). RNA integrity was confirmed by 1.5% agarose gel electrophoresis. RNA sequencing was performed by GENEWIZ (Suzhou, China). Raw sequencing data were filtered by Trimmomatic (version 0.36) and the clean reads were mapped to the reference genome of mouse (mm10) using STAR software (version 2.5.3a) with default parameters. Reads mapped to the exon regions were counted using *featureCounts* (Subread-1.5.1, Bioconductor). The resulting BAM files were sorted and indexed using SAMtools⁵².

Differential expression analysis was performed using DESeq2 (version 1.32.0). Genes with expression showing $|\log_2 \text{fold change}| \geq 1$ and adjust $P < 0.05$ were assigned as differentially expressed genes (DEGs). Gene Ontology Biological Process (GOBP) enrichment analysis and KEGG analysis were conducted using DAVID (<https://david.ncifcrf.gov/>). All GO and KEGG terms presented in this study have P value lower than 0.05.

Apical resection (AR) in mouse hearts

AR was carried out in P1 and P8 mice hearts as described⁵³. Briefly, mice were anesthetized by ice freezing for 2–5 min. A left parasternal thoracotomy at the fourth intercostal space was performed using blunt scissors to expose the heart. A modified 10 μL pipette tip, connected to a vacuum pump operating at 0.06 ± 0.005 MPa, was gently applied to the apex of the left ventricle for approximately 12 s. The apex was then dissected with a single incision adjacent to the pipette tip trails using iridectomy scissors. The chest and skin incision were sutured with 7-0 silk suture. Post-operative mice were placed on the 37 $^{\circ}\text{C}$ heating pad until recovery. Sham controls underwent the same procedures without apex amputation.

Animals were randomly assigned to experimental groups before surgery. All surgery operations were performed in a double-blinded manner.

Adult mouse model of myocardial infarction (MI)

MI was performed in 8-week-old C57BL/6 mice, including *LncBAR*^{-/-} mice and WT mice. Before surgery, mice were anesthetized by intraperitoneal

injection of a mixture of tribromoethanol (320 mg/kg) and 2-butanol (160 mg/kg). After exposing the heart, myocardial infarction was induced by permanent ligation of the left anterior descending artery (LAD) with a 7-0 polypropylene suture. Sham-operated animals served as surgical controls and were subjected to the same procedures as the experimental animals with the exception that the LAD was not ligated. Mice were allowed to recover using a mouse ventilator and heating pad.

Animals were randomly assigned to experimental groups before surgery. All surgery operations were performed in a double-blinded manner.

Adeno-associated virus of serotype 9 (AAV9) packaging and delivery

The *LncBAR* sequence was cloned into the AAV9 plasmid (pcAAV-cTnT-GdGreen-WPRE), with transgene expression driven by the cTnT promoter. Viral particles were produced by OBiO Biotechnology Co. Ltd., Shanghai, China. Neonatal AAV9-mediated *LncBAR* overexpression was achieved through direct injection into the cardiac ventricles using an insulin syringe with a 30-gauge needle, at a dose of 5×10^{10} vector genomes per animal. For viral transduction in adult mice post-MI, 5×10^{11} vector genomes per animal were intramyocardially injected into the boundary between the border and infarct zones of infarcted hearts. All viral inoculation were performed in a double-blinded manner.

Histological analysis

For immunohistochemistry, mouse hearts were fixed with 0.5% PFA in PBS supplemented with 5% sucrose overnight. After sequential dehydration with sucrose, samples were embedded in OCT (Sakura, 4583) and slowly frozen in isopropanol on ice. The hearts were vertically sectioned into 5 μ m cryosections and stained with antibodies listed in Supplementary Table 2, and subsequently underwent DAPI staining. Tissue sections were imaged using a Leica confocal microscope, and measurements were conducted in a double-blinded manner.

For Masson's trichrome staining, mouse hearts were perfused with 10 mM KCl until arrested, followed by perfusion with DPBS and 4% PFA. After embedded in paraffin, the samples were vertically sectioned into 5 μ m sections, deparaffinized, and stained using the Masson's trichrome staining kit (Baso, BA4079B) according to the manufacturer's instructions. Fibrotic area was calculated as the percentage of total fibrotic area relative to total heart section area.

Echocardiography

Adult mice were subjected to 1–2% isoflurane as anesthesia for 3–5 min for echocardiography. Echocardiography was performed using VINNO 6 VET (VINNO Corporation). M-mode imaging was used to measure left ventricular end-systolic anterior wall thickness and to calculate the ejection fraction and fractional shortening. All echocardiography was performed in a double-blinded manner.

Statistical analysis

Data were analyzed and plotted using GraphPad Prism v8 (GraphPad Software) and FlowJo v10 (BD Biosciences). All results were expressed as mean \pm SEM. The two-tailed unpaired *t* test was used to determine the significance of differences between two groups. One-way or two-way analysis of variance (ANOVA) was used to determine the significance of experiments containing three or more conditions. In all cases, $P < 0.05$ was considered statistically significant ($*P < 0.05$; $**P < 0.01$; $***P < 0.001$). All data are representative of multiple repeated experiments.

Data availability

RNA-seq dataset in this study has been deposited in NCBI Gene Expression Omnibus with the accession code GSE279692 and is publicly available as of the date of publication. All the data and bioinformatic analysis can be obtained from the corresponding author upon reasonable request. The BRG1 ChIP-seq data were obtained from GEO (ncbi.nlm.nih.gov/geo/) (GSE249559) ref³¹.

Received: 17 February 2025; Accepted: 3 October 2025;

Published online: 17 November 2025

References

- Puente, B. N. et al. The oxygen-rich postnatal environment induces cardiomyocyte cell-cycle arrest through DNA damage response. *Cell* **157**, 565–579 (2014).
- Mohamed, T. M. A. et al. Regulation of cell cycle to stimulate adult cardiomyocyte proliferation and cardiac regeneration. *Cell* **173**, 104–116.e112 (2018).
- Chen, Y. et al. Reversible reprogramming of cardiomyocytes to a fetal state drives heart regeneration in mice. *Science* **373**, 1537–1540 (2021).
- Nishiyama, C. et al. Prolonged myocardial regenerative capacity in neonatal opossum. *Circulation* **146**, 125–139 (2022).
- Porrello, E. R. et al. Transient regenerative potential of the neonatal mouse heart. *Science* **331**, 1078–1080 (2011).
- Payan, S. M., Hubert, F. & Rochais, F. Cardiomyocyte proliferation, a target for cardiac regeneration. *Biochim. Biophys. Acta Mol. Cell Res.* **1867**, 118461 (2020).
- Mahmoud, A. I. et al. Meis1 regulates postnatal cardiomyocyte cell cycle arrest. *Nature* **497**, 249–253 (2013).
- Tian, Y. et al. A microRNA-Hippo pathway that promotes cardiomyocyte proliferation and cardiac regeneration in mice. *Sci. Transl. Med.* **7**, 279ra238 (2015).
- Chen, J. et al. mir-17-92 cluster is required for and sufficient to induce cardiomyocyte proliferation in postnatal and adult hearts. *Circ. Res.* **112**, 1557–1566 (2013).
- Bersell, K., Arab, S., Haring, B. & Kuhn, B. Neuregulin1/ ErbB4 signaling induces cardiomyocyte proliferation and repair of heart injury. *Cell* **138**, 257–270 (2009).
- Mashtair, N. et al. Modular organization and assembly of SWI/SNF family chromatin remodeling complexes. *Cell* **175**, 1272–1288.e1220 (2018).
- Bultman, S. et al. A Brg1 null mutation in the mouse reveals functional differences among mammalian SWI/SNF complexes. *Mol. Cell* **6**, 1287–1295 (2000).
- Stankunas, K. et al. Endocardial Brg1 represses ADAMTS1 to maintain the microenvironment for myocardial morphogenesis. *Dev. Cell* **14**, 298–311 (2008).
- Hang, C. T. et al. Chromatin regulation by Brg1 underlies heart muscle development and disease. *Nature* **466**, 62–67 (2010).
- Liu, X. et al. BRG1 protects the heart from acute myocardial infarction by reducing oxidative damage through the activation of the NRF2/HO1 signaling pathway. *Free Radic. Biol. Med.* **160**, 820–836 (2020).
- Xiao, C. et al. Chromatin-remodelling factor Brg1 regulates myocardial proliferation and regeneration in zebrafish. *Nat. Commun.* **7**, 13787 (2016).
- Statello, L., Guo, C. J., Chen, L. L. & Huarte, M. Gene regulation by long non-coding RNAs and its biological functions. *Nat. Rev. Mol. Cell Biol.* **22**, 96–118 (2021).
- Yin, Q., Wu, A. & Liu, M. Plasma long non-coding RNA (lncRNA) GAS5 is a new biomarker for coronary artery disease. *Med. Sci. Monit.* **23**, 6042–6048 (2017).
- Liu, S. D. et al. GAS5 promotes myocardial apoptosis in myocardial ischemia-reperfusion injury via upregulating LAS1 expression. *Eur. Rev. Med. Pharm. Sci.* **22**, 8447–8453 (2018).
- Lv, F., Liu, L., Feng, Q. & Yang, X. Long non-coding RNA MALAT1 and its target microRNA-125b associate with disease risk, severity, and major adverse cardiovascular event of coronary heart disease. *J. Clin. Lab. Anal.* **35**, e23593 (2021).
- Zhang, L. et al. H19 knockdown suppresses proliferation and induces apoptosis by regulating miR-148b/WNT/ β -catenin in ox-LDL-stimulated vascular smooth muscle cells. *J. Biomed. Sci.* **25**, 11 (2018).

22. Chen, D., Zhang, Z., Lu, X. & Yang, X. Long non-coding RNA SNHG15 regulates cardiomyocyte apoptosis after hypoxia/reperfusion injury via modulating miR-188-5p/PTEN axis. *Arch. Physiol. Biochem.* **129**, 283–290 (2023).
23. Liu, L. et al. The H19 long noncoding RNA is a novel negative regulator of cardiomyocyte hypertrophy. *Cardiovasc. Res.* **111**, 56–65 (2016).
24. Wang, A. et al. An epigenetic circuit controls neurogenic programs during neocortex development. *Development* **148**, dev199772 (2021).
25. Ponnusamy, M. et al. Long noncoding RNA CPR (Cardiomyocyte Proliferation Regulator) regulates cardiomyocyte proliferation and cardiac repair. *Circulation* **139**, 2668–2684 (2019).
26. Ji, X. et al. Sphingolipid metabolism controls mammalian heart regeneration. *Cell Metab.* **36**, 839–856.e838 (2024).
27. Lei, I., Tian, S., Chen, V., Zhao, Y. & Wang, Z. SWI/SNF component BAF250a coordinates OCT4 and WNT signaling pathway to control cardiac lineage differentiation. *Front. Cell Dev. Biol.* **7**, 358 (2019).
28. Sharma, T., Olea-Flores, M. & Imbalzano, A. N. Regulation of the Wnt signaling pathway during myogenesis by the mammalian SWI/SNF ATPase BRG1. *Front. Cell Dev. Biol.* **11**, 1160227 (2023).
29. Ghafouri-Fard, S. et al. Interplay between PI3K/AKT pathway and heart disorders. *Mol. Biol. Rep.* **49**, 9767–9781 (2022).
30. Lei, Y. Q. et al. Nono deficiency impedes the proliferation and adhesion of H9c2 cardiomyocytes through Pi3k/Akt signaling pathway. *Sci. Rep.* **13**, 7134 (2023).
31. Kang, Q. et al. BRG1 promotes progression of B-cell acute lymphoblastic leukemia by disrupting PPP2R1A transcription. *Cell Death Dis.* **15**, 621 (2024).
32. Mably, J. D. & Wang, D. Z. Long non-coding RNAs in cardiac hypertrophy and heart failure: functions, mechanisms and clinical prospects. *Nat. Rev. Cardiol.* **21**, 326–345 (2024).
33. Rayner, K. J. & Liu, P. P. Long noncoding RNAs in the heart: the regulatory roadmap of cardiovascular development and disease. *Circ. Cardiovasc. Genet.* **9**, 101–103 (2016).
34. Li, M. et al. LncRNA Snhg1-driven self-reinforcing regulatory network promoted cardiac regeneration and repair after myocardial infarction. *Theranostics* **11**, 9397–9414 (2021).
35. Yijian, L. et al. CircNXC1 modulates cardiomyocyte proliferation through promoting ubiquitination of BRG1. *Cell Signal.* **120**, 111193 (2024).
36. Lin, H. et al. Antihypertrophic memory after regression of exercise-induced physiological myocardial hypertrophy is mediated by the long noncoding RNA Mhrt779. *Circulation* **143**, 2277–2292 (2021).
37. Lin, Z. et al. Pi3kcb links Hippo-YAP and PI3K-AKT signaling pathways to promote cardiomyocyte proliferation and survival. *Circ. Res.* **116**, 35–45 (2015).
38. Beigi, F. et al. C3orf58, a novel paracrine protein, stimulates cardiomyocyte cell-cycle progression through the PI3K-AKT-CDK7 pathway. *Circ. Res.* **113**, 372–380 (2013).
39. Feng, J. et al. Versican promotes cardiomyocyte proliferation and cardiac repair. *Circulation* **149**, 1004–1015 (2024).
40. Xin, M. et al. Regulation of insulin-like growth factor signaling by Yap governs cardiomyocyte proliferation and embryonic heart size. *Sci. Signal.* **4**, ra70 (2011).
41. Johnson, J., Mohsin, S. & Houser, S. R. Cardiomyocyte proliferation as a source of new myocyte development in the adult heart. *Int. J. Mol. Sci.* **22**, 7764 (2021).
42. Auchampach, J. et al. Measuring cardiomyocyte cell-cycle activity and proliferation in the age of heart regeneration. *Am. J. Physiol. Heart Circ. Physiol.* **322**, H579–h596 (2022).
43. Zong, H., Espinosa, J. S., Su, H. H., Muzumdar, M. D. & Luo, L. Mosaic analysis with double markers in mice. *Cell* **121**, 479–492 (2005).
44. Wang, L. et al. Down-regulation of Beclin1 promotes direct cardiac reprogramming. *Sci. Transl. Med.* **12**, eaay7856 (2020).
45. Liu, Z. et al. Single-cell transcriptomics reconstructs fate conversion from fibroblast to cardiomyocyte. *Nature* **551**, 100–104 (2017).
46. Bell, R. M., Mocanu, M. M. & Yellon, D. M. Retrograde heart perfusion: the Langendorff technique of isolated heart perfusion. *J. Mol. Cell Cardiol.* **50**, 940–950 (2011).
47. Wang, L. et al. Stoichiometry of Gata4, Mef2c, and Tbx5 influences the efficiency and quality of induced cardiac myocyte reprogramming. *Circ. Res.* **116**, 237–244 (2015).
48. Sokol, L. et al. Protocols for endothelial cell isolation from mouse tissues: small intestine, colon, heart, and liver. *STAR Protoc.* **2**, 100489 (2021).
49. Chen, X. et al. QKI is a critical pre-mRNA alternative splicing regulator of cardiac myofibrillogenesis and contractile function. *Nat. Commun.* **12**, 89 (2021).
50. Lian, X. et al. Directed cardiomyocyte differentiation from human pluripotent stem cells by modulating Wnt/ β -catenin signaling under fully defined conditions. *Nat. Protoc.* **8**, 162–175 (2013).
51. Gao, R. et al. Long noncoding RNA cardiac physiological hypertrophy-associated regulator induces cardiac physiological hypertrophy and promotes functional recovery after myocardial ischemia-reperfusion injury. *Circulation* **144**, 303–317 (2021).
52. Li, H. et al. The sequence alignment/map format and SAMtools. *Bioinformatics* **25**, 2078–2079 (2009).
53. Bei, Y. et al. A modified apical resection model with high accuracy and reproducibility in neonatal mouse and rat hearts. *NPJ Regen. Med.* **8**, 9 (2023).

Acknowledgements

We thank the core facility of the Medical Research Institute at Wuhan University for their technical support. We thank members of the Wang and Cheng laboratories for helpful discussions and critical reviews of the manuscript. We thank Dr. Yanggan Wang (Wuhan University) for providing technique supports. This work was supported by National Key Research and Development Program of China (2021YFA1102500), National Natural Science Foundation of China (32470787, 92068107 and 32070728), Fundamental Research Funds for the Central Universities in China (2042022kf0052, 2042022dx0003), Natural Science Foundation of Hubei Province (2023AFA059), and the Major Scientific and Technological Project of Hubei Province (2022ACA005) to Li Wang. Dr. Yan Zhou was supported by grants from National Key R&D Program of China (2022YFA0806603), and National Natural Science Foundation of China (32270876). The authors have reported that they have no relationships relevant to the contents of this paper to disclose.

Author contributions

J.L. designed and performed experiments, analyzed data and wrote the manuscript. H.C. performed the animal experiments. Y.C. and R.P. performed histological analysis. L.X. performed CM differentiation from human ES cells. Z.L., Y.Z., and L.W. conceived and supervised the study, designed the experiments, analyzed data and wrote the manuscript. Y.Z. and L.W. provided the funding.

Competing interests

The authors declare no competing interests.

Additional information

Supplementary information The online version contains supplementary material available at <https://doi.org/10.1038/s41536-025-00439-6>.

Correspondence and requests for materials should be addressed to Zhibing Lu, Yan Zhou or Li Wang.

Reprints and permissions information is available at <http://www.nature.com/reprints>

Publisher's note Springer Nature remains neutral with regard to jurisdictional claims in published maps and institutional affiliations.

Open Access This article is licensed under a Creative Commons Attribution-NonCommercial-NoDerivatives 4.0 International License, which permits any non-commercial use, sharing, distribution and reproduction in any medium or format, as long as you give appropriate credit to the original author(s) and the source, provide a link to the Creative Commons licence, and indicate if you modified the licensed material. You do not have permission under this licence to share adapted material derived from this article or parts of it. The images or other third party material in this article are included in the article's Creative Commons licence, unless indicated otherwise in a credit line to the material. If material is not included in the article's Creative Commons licence and your intended use is not permitted by statutory regulation or exceeds the permitted use, you will need to obtain permission directly from the copyright holder. To view a copy of this licence, visit <http://creativecommons.org/licenses/by-nc-nd/4.0/>.

© The Author(s) 2025